

Appendix E

FCT Document Cover Sheet

Waste Form Degradation Model Status Report: Electrochemical Model
for Used Fuel Matrix Degradation Rate

Name/Title of Deliverable/Milestone
Work Package Title and Number

EBS Evaluations-ANL FT-12AN080601

Work Package WBS Number

1.02.08.06

Milestone Number

M3FT-12AN080601

Responsible Work Package Manager

William L. Ebert

(Name/Signature)

August 9, 2012

(Date Submitted)

Quality Rigor Level for Deliverable/Milestone	<input checked="" type="checkbox"/> QRL-3	<input type="checkbox"/> QRL-2	<input type="checkbox"/> QRL-1 <input type="checkbox"/> Nuclear Data	<input type="checkbox"/> N/A*
---	---	--------------------------------	---	-------------------------------

This deliverable was prepared in accordance with

Argonne National Laboratory

(Participant/National Laboratory Name)

QA program which meets the requirements of

DOE Order 414.1

NQA-1-2000

Other: _____

This Deliverable was subjected to:

Technical Review

Peer Review

Technical Review (TR)

Peer Review (PR)

Review Documentation Provided

Review Documentation Provided

Signed TR Report, or

Signed PR Report, or

TR Report No.: _____

PR Report No.: _____

Signed TR Concurrence Sheet (attached), or

Signed PR Concurrence Sheet (attached), or

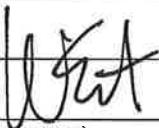
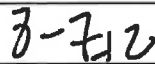
Signature of TR Reviewer(s) below

Signature of PR Reviewers below

Name and Signature of Reviewers

William L. Ebert

8/7/2012

(Name/Signature)

(Date)

*Note: In some cases there may be a milestone where an item is being fabricated, maintenance is being performed on a facility, or a document is being issued through a formal document control process where it specifically calls out a formal review of the document. In these cases, documentation (e.g., inspection report, maintenance request, work planning package documentation, or the documented review of the issued document through the document control process) of the completion of the activity along with the Document Cover Sheet is sufficient to demonstrate achieving the milestone. QRL for such milestones may also be marked N/A in the work package provided the work package clearly specifies the requirement to use the Document Cover Sheet and provide supporting documentation.

***Waste Form Degradation
Model Status Report:
Electrochemical Model for
Used Fuel Matrix
Degradation Rate***

**Used Fuel Disposition –
Engineered Barrier Systems**

***Prepared for
U.S. Department of Energy
Used Fuel Disposition Campaign***

James Jerden

Kurt Frey

Terry Cruse

William Ebert

Argonne National Laboratory

August 9, 2012

FCRD-UFD-2012-000169



This work was supported by the US Department of Energy, Office of Nuclear Energy. The report was prepared at Argonne National Laboratory as part of the Used Fuel Disposition (UFD) Generic Engineered Barrier Systems (EBS) Evaluations [National Technical Director Peter Swift (SNL)]. This report is submitted for milestone M3FT-12AN0806013 for the work package: FT-12AN080601.

Government License Notice: The submitted manuscript has been created by UChicago Argonne, LLC, Operator of Argonne National Laboratory (“Argonne”). Argonne, a U.S. Department of Energy Office of Science laboratory, is operated under Contract No. DE-AC02-06CH11357. The U.S. Government retains for itself, and others acting on its behalf, a paid-up nonexclusive, irrevocable worldwide license in said article to reproduce, prepare derivative works, distribute copies to the public, and perform publicly and display publicly, by or on behalf of the Government.

This work was supported by the U.S. Department of Energy, Office of Nuclear Energy, under Contract DE-AC02-06CH11357.

DISCLAIMER

This information was prepared as an account of work sponsored by an agency of the U.S. Government. Neither the U.S. Government nor any agency thereof, nor any of their employees, makes any warranty, expressed or implied, or assumes any legal liability or responsibility for the accuracy, completeness, or usefulness, of any information, apparatus, product, or process disclosed, or represents that its use would not infringe privately owned rights. References herein to any specific commercial product, process, or service by trade name, trade mark, manufacturer, or otherwise, does not necessarily constitute or imply its endorsement, recommendation, or favoring by the U.S. Government or any agency thereof. The views and opinions of authors expressed herein do not necessarily state or reflect those of the U.S. Government or any agency thereof.

SUMMARY

This work is being performed as part of the DOE NE Used Fuel Disposition (UFD) Campaign Engineered Barrier Systems (EBS) Evaluations project work package: FT-12AN080601. This document was prepared to meet milestone M3FT-12AN0806013. The overall objective of this work is to develop a predictive model for the degradation of used uranium oxide fuel based on fundamental electrochemical and thermodynamic principles that can be used to provide a source term for radionuclide release in disposal system performance assessments. This involves quantifying the contributions of all processes affecting the corrosion potential at the used fuel surface, including processes that have not been taken into account in other electrochemical models for used fuel degradation, such as the role surface phases catalyzing redox reactions. The approach is to extend an existing model that is based on the electrochemical mixed potential theory to include the role of (H_2) as a reducing agent, the effects of redox reactions that are catalyzed by noble metal particles (NMPs), interactions with engineering materials, the evolving geometry of the corroding fuel grains, and other factors to represent the disposal environments being evaluated by DOE. Work in FY 2012 was focused on implementing the Canadian-mixed potential model (Canadian-MPM) for UO_2 fuel dissolution (King and Kolar, 1999, King and Kolar, 2003, Shoosmith et al., 2003) using MATLAB scripts. This provided a working model that was used to demonstrate the efficacy of our approach and provide initial guidance to the experimental work. The initial version of the MATLAB implementation of mixed potential model, referred to as the ANL-MPM Version 1, was produced as a base model and verified by reproducing published results from the Canadian-MPM reports. The model is being rewritten and extended to include the additional reactions and processes affecting fuel dissolution that are listed above.

The specific objectives for this project that have been achieved this year (FY-2012) and are discussed in this report are as follows:

- Implementation, using our own scripts/code, of an established and well documented used fuel degradation model (Canadian-mixed potential model) that is based on mixed potential theory.
- Verification of our scripting and coding by reproducing published results from the Canadian model.
- Performance of sensitivity analyses to determine which model parameters and input variables have the strongest impact on the calculated used fuel degradation rate.
- Completion of a critical review of the sources of all model parameters and input variables to determine which values need further investigation through literature review or experimental studies. This review also identified which variables must be provided by other process models.
- Extension of the base-case model to quantitatively include reactions involving dissolved hydrogen that may protect used fuel from oxidative dissolution by lowering the electrochemical potential at the fuel surface.
- Development of a plan to extend the base-case model to account for the catalytic effects of fission product alloy phases (noble metal particles) on reactions affecting UO_2 dissolution, such as the kinetic balance of H_2 oxidation and H_2O_2 reduction reactions.

The ANL-MPM Version 1 is a 1-dimensional reaction-diffusion model that accounts for the following processes:

- Interfacial redox reaction kinetics (oxidative dissolution of UO_2 matrix).
- Chemical or solubility based dissolution of the fuel matrix.
- Complexation of uranium at the fuel surface and in the bulk solution by carbonate.
- The production of hydrogen peroxide (the dominant fuel oxidant in anoxic repository environments) by alpha-radiolysis.
- Diffusion of reactants and products in the groundwater away from and towards the reacting fuel surface.
- The precipitation and dissolution of a U(VI) corrosion product layer on the fuel surface.
- Adsorption of uranium onto iron oxides.
- All interfacial and bulk reactions have a built in Arrhenius-type temperature dependence.

Version 1 has been completed and will be used as a baseline check for future versions. An initial working beta version of the ANL-MPM Version 2 is being written as an extension of ANL-MPM Version 1 to include the following processes and conditions:

- Quantify the oxidation of dissolved H_2 at the used fuel/solution interface: H_2 concentration to be supplied by other EBS model or user specified).
- Represent the NMPs as a separate domain at the used fuel/solution interface. The "size" of the NMP domain (relative to the fuel) is specified by the user in terms of a surface coverage and is electrically linked with the UO_2 matrix by a user adjustable resistance term. This will allow the effects of NMP corrosion and the sorption of catalytic poisons on the efficiency of the redox reactions to be taken into account.
- Quantify the bulk decomposition of hydrogen peroxide (with temperature dependence).
- Provide option for user to specify temperature and dose profiles of the fuel (profiles can be constant single values or functions).
- Include rapid diffusion option to facilitate the calculation of concentrations of species with diffusion coefficients sufficiently large that steady state is reached within days. This decreases the computer time needed for model convergence and makes for more efficient evaluations of long-term behavior.

Version 2 will be further developed in FY 2013 to add additional capabilities, such as calculation of the evolving surface area as the matrix particles corrode, groundwater penetrates grain boundaries, and alteration phases precipitate. An important aspect of the work planned for FY 2013 is integration of the experimental results into the model. This will include refinements of the kinetic parameters used to model key redox reactions and UO_2 dissolution over a range of solution compositions and the effects of NMP corrosion. Because the ANL-MPM is based on fundamental principles, it is flexible enough to be applied to a range of chemical environments. In this report, we identify the model parameters that are sensitive to the environment and must be determined to apply the ANL-MPM to the full range of repository scenarios being considered as part of the UFD campaign (i.e., those in granite, basalt, clay/shale, salt, and rhyolite environments). On-going experimental work described in Jerden et al., 2012 and Ebert et al., 2012 is focused on providing key model parameter values that are needed to improve the predictive accuracy and capabilities of the ANL-MPM.

CONTENTS

SUMMARY	i
ACRONYMS.....	vi
1. INTRODUCTION AND BACKGROUND	1
1.1. Objectives and Scope.....	1
1.2. Used Fuel Microstructure and Radionuclide Distribution.....	2
1.3. Fuel Matrix Degradation Process	3
1.4. Modeling Approach: Implementation of a Mixed Potential Model for Matrix Degradation.....	7
1.5.. Canadian Mixed Potential Model (Canadian-MPM).....	8
1.6. Interface with Generic Performance Assessment Models	10
2. ANL IMPLEMENTATION OF THE CANADIAN MIXED POTENTIAL MODEL: ANL-MPM VERSION 1.....	12
2.1. Parameter Database for ANL-MPM Version 1	12
2.2. Governing Equations and Fundamental Electrochemical Relationships Used in Mixed Potential Model Implementation.....	20
2.3. Radiolysis Model Included in the ANL-MPM Version 1	24
2.4. Verification of ANL-MPM Version 1 and Sensitivity Studies of Selected Parameters.....	29
2.5. Example Calculation of Used Fuel Matrix Degradation Rate Using the ANL-MPM.....	34
2.6. Uncertainty and Conditional Applicability of the ANL-MPM.....	36
3. ANL-MPM VERSION 2	37
4. SUMMARY AND FUTURE WORK	41
REFERENCES CITED AND CONSULTED	43

FIGURES

Figure 1. Optical micrographs of a polished used fuel cross-section showing the distinct microstructural regions that influence degradation and radionuclide release (Tsai 2003). This sample was cut from an H. B. Robinson PWR Rod with a burnup of 67 GWd/MTU.....	3
Figure 2. Experimental results from Röllin et al., 2001 showing that the dissolution rate of the UO_2 matrix of used fuel decreases by nearly three orders of magnitude when chemical dissolution vs. oxidative dissolution is the dominant degradation process.	4
Figure 3. Schematic diagram identifying key surface processes involved in the degradation of used fuel (adapted from Shoesmith, 2007).....	5
Figure 4. Simplified representation of breached canister system used in Shoesmith et al. (2003) MPM for the oxidative degradation of UO_2 fuel due to alpha radiolysis of water.	9
Figure 5. Reaction scheme used in the Shoesmith et al. (2003) (Canadian-MPM) for the oxidative degradation of UO_2 fuel due to alpha radiolysis of water (key half-reactions listed below). Aqueous species are shown in blue, dotted lines represent diffusive fluxes. The “k” labels represent rate expressions for the individual half-reactions. Reactions labeled with letters are for heterogeneous (surface) processes and those labeled with numbers describe homogeneous processes. Anodic reactions are noted with yellow or orange arrows and the cathodic reactions are shown in blue arrows. “ads” stands for adsorbed.	10
Figure 6. Simplified algorithm for the evolution of the used fuel corrosion potential and interfacial reaction rates with time as calculated by the ANL-MPM Version 1: see Table 3 for concentration input sources.....	18
Figure 7. Schematic representation of mixed potential model grid spacing between the used fuel and steel surface boundaries (not all spacings are shown). Spacing is logarithmic with finer intervals at the two interfaces. The current implementation of the ANL-MPM Version 1 contains 250 grid points with a minimum grid spacing of 1 micrometers and a maximum spacing of 1000 micrometers.	19
Figure 8. Schematic drawing of the alpha-radiation regions within the ANL-MPM Version 1. See Table 5 and section 2.3. for discussion.....	27

Figure 9. ANL-MPM Version 1 example calculations showing how dose rate and the presence of a U(VI) alteration layer effects the concentration of radiolytic H₂O₂ and the associated fuel corrosion potential and matrix dissolution rate. For these model runs the starting concentrations of carbonate and dissolved oxygen were 1x10⁻⁵ molar and 1x10⁻⁶ molar respectively and the temperature was a constant 30°C.....29

Figure 10. Comparison of results from the ANL-MPM, MATLAB scripts (colored lines) with results from the Canadian-MPM (black line) and experimental results from King and Kolar (2002).....32

Figure 11. Comparison of results from the ANL-MPM, MATLAB scripts (colored lines) with results from the Canadian-MPM (black lines) and experimental results from King and Kolar (2002).....32

Figure 12. Comparison of results from the ANL-MPM, MATLAB scripts (colored lines) with results from the Canadian-MPM (black line) and experimental results from King and Kolar (2002).....33

Figure 13. Comparison of results from the ANL-MPM, MATLAB scripts (colored lines) with results from the Canadian-MPM (black line).33

Figure 14. Dissolution rate of uranium dioxide in mg per day per square meter of exposed fuel calculated using the ANL-MPM Version 1 for one millimolar dissolved carbonate (constant) and initial dissolved oxygen concentration of 1x10⁻⁶ molar. The temperature and dose profiles used for this calculation are shown in Figure 15.34

Figure 15. Time dependence of alpha-dose rate in water layer adjacent to used fuel (top) and fuel surface temperature (bottom) used in the example dissolution rate calculation shown in Figure 14. The dose and temperature profiles are from King and Kolar (1999).....35

Figure 16. Simplified reaction scheme (not showing all component fluxes) used in the ANL-MPM modified to include catalytic roles of NMP.39

Figure 17. Schematic representation highlighting the process of interest for the ANL study (top) and the basic experimental approach that will be used (bottom).....40

TABLES

Table 1.	Part of the ANL-MPM parameter database: interfacial reactions for UO ₂ matrix dissolution. See Figure 4 for coupling between reactions	13
Table 2.	Part of the ANL-MPM parameter database: homogeneous reactions. See Figure 4 for coupling between reactions.	14
Table 3.	Part of the ANL-MPM parameter database: components (species) included in mass balance equations (see examples Eq.21 – Eq.25). The concentration column (C _i) identifies links to other UFD process models that are being or will be developed as part of the FY-2013 research and development activities (IPC: in-package-chemistry model).....	15
Table 4.	Part of the ANL-MPM parameter database: physical parameters used in electrochemical and mass balance equations (Eq.1 – Eq.25).....	16
Table 5.	Part of the ANL-MPM parameter database: parameters and variables used in the radiolysis sub-model (see Figures 7 and section 2.4. for discussion).....	17
Table. 6.	Typical range of activation energy (ΔH) values for selected chemical processes (Langmuir, 1997, page 62).....	18
Table 7.	Extension of ANL-MPM parameter database to account for oxidation and reduction reactions that may be catalyzed on noble metal particle surfaces.....	38

ACRONYMS

ANL	Argonne National Laboratory
DOE NE	Department of Energy Nuclear Energy
EBS	Engineered Barrier System
GPAM	Generic Performance Assessment Model
GSPM	Generic System Performance Model
MPM	Mixed Potential Model
NMP	Noble Metal bearing Particle
UFD	Used Fuel Disposition
UOX	Uranium Oxide Fuel
MOX	Mixed Oxide Fuel

Electrochemical Model for Used Fuel Matrix Degradation Rate

1. INTRODUCTION AND BACKGROUND

This work was performed as part of the DOE NE Used Fuel Disposition (UFD) Campaign's Engineered Barrier Systems (EBS) Evaluations, work package: FT-12AN080601. This document represents the August 9, 2012 milestone report: M3FT-12AN0806013.

1.1. Objectives and Scope

The overall objective of this work is to develop a predictive model for the degradation of used uranium oxide fuel that is based on fundamental electrochemical and thermodynamic principles. It is anticipated that this process model will provide the fractional degradation rate of used fuel and the radionuclide source terms as direct inputs to the UFD Generic Performance Assessment Model (GPAM) that is currently being implemented to evaluate high-level waste disposal systems (e.g., Geoff Freeze, 2012, Advanced Implementation of the UFD Generic Performance Assessment Model, presentation at Used Fuel Disposition Working Group Meeting, May 16, 2012, Las Vegas, NV).

Our approach is to tailor the Mixed Potential Model (MPM) for UO_2 matrix dissolution that was developed as part of the Canadian repository program (Canadian-MPM) for application to US disposal systems and to extend the model to include process that affect the fuel dissolution rate that were not included in the original Canadian model. The most important processes that are being incorporated into the ANL mixed potential model (ANL-MPM) are: (1) the role of hydrogen oxidation at the used fuel interface and (2) the catalysis of oxidation/reduction reactions (hydrogen oxidation, hydrogen peroxide, oxygen reduction) by noble metal bearing particles (NMP) on the fuel surface (also referred to as the epsilon phase or the fission product alloy phase), and (3) the effects of long-term corrosion on poisons on the catalytic efficiency of the NMPs. Other additions being made are options to accelerate diffusion processes to facilitate modeling long-term behavior, evolution of the fuel surface area during grain boundary and matrix dissolution, and specification of the NMP surface area.

Our modeling approach was divided into two stages: (1) implementation of the Canadian-MPM in the programming language MATLAB with only minor changes to the original model. The scripts resulting from this work are referred to as the ANL-MPM Version 1. (2) Extension and optimization of the MPM implemented in MATLAB. This model, which is still under development, is referred to as the ANL-MPM Version 2. The Version 2 of the ANL-MPM quantifies the effects of dissolved hydrogen and the catalytic properties of NMP on fuel matrix dissolution. It has been optimized from a computing standpoint by using a rapid diffusion approach which significantly decreases the time it takes for the model to converge on a unique solution and facilitates calculations of long-term behavior.

Sensitivity studies of the ANL-MPM Version 1 have been used to identify key model parameters for which values must be determined from literature data, measured experimentally, or calculated

with submodels, such as the concentrations of radiolytic products, for application to conditions other than those used in the Canadian model. The focus of our model sensitivity studies and linked experimental work is on demonstrating and improving the applicability of the ANL-MPM to the full range of generic repository concepts being considered as part of the UFD campaign.

The on-going experimental program is designed to support model development (i.e., measure the key electrochemical and reaction kinetic parameters identified in the model sensitivity studies) and is summarized below and described in more detail in Jerden et al., 2012. Results from the first sets of ANL electrochemical experiments are presented in Ebert et al., 2012 (in preparation).

1.2. Used Fuel Microstructure and Radionuclide Distribution

The chemical state and distribution of fission product elements in irradiated used fuels have been studied using thermodynamic calculations and experimental measurements (Dehaut 2001). In used fuels the oxygen potential is less than approximately -400 kJ/mol (Dehaut 2001). Under these very low oxygen potential conditions uranium in the used fuel matrix is present mostly in the U(IV) oxidation state. Likewise, the other radionuclides in the fuel matrix are in low or zero valent states (Kleykamp 1985). The noble transition metal fission products are present in metallic (zero valent) form and accumulate along with a fraction of the molybdenum and technetium inventories within grain boundaries and fractures as they exsolve from the fuel matrix grains during burnup (Kleykamp 1985). The fact that the fuel matrix elements and radionuclides are present in the fuel in lower valence (and less soluble) states is important because degradation and mobilization will be a slow process unless both the fuel matrix and the associated radionuclides become oxidized under the disposal conditions. The combined processes of oxidation and dissolution of the oxide is referred to as oxidative dissolution. *The electrochemical model that was implemented as part of the present study (ANL-MPM) accounts for the rate of oxidative dissolution of the used fuel matrix and thus can be used to predict an overall radionuclide release rate.*

As the fuel is burned in the reactor, most fission product and neutron capture elements are retained within the fluorite lattice structure of the fuel matrix. However, because some of the fission product elements are not soluble in the UO₂ matrix, a fraction of the inventory of these elements migrates out of the fuel grains under normal reactor operating conditions and accumulates at the grain boundaries (Pelletier 2001). The extent of migration of these fission products out of the fuel grains and the subsequent accumulation at the grain boundaries and in gap regions of the fuel depends on the diffusion coefficients of the individual fission product elements in the used fuel matrix and the available mechanisms for migration. The distribution of radionuclides in a used fuel rod strongly depends on the thermal history and burnup conditions of the fuel (Pelletier 2001).

Like the fission gasses, some of the fission product cesium and iodine diffuses out of the fuel grains and is found at the grain boundaries and in the gap region between the fuel pellets and the cladding (Dehaut 2001). After irradiation, part of the fission product molybdenum, ruthenium, technetium, rhodium, and palladium inventory is found in the form of metallic alloy particles located within the fuel grains and at grain boundaries. In this report, these fission product alloy phases are referred to as the Noble Metal bearing Particles (NMP); they are also referred to as

epsilon phase particles in the general literature. The accumulation of NMP is more evident in the higher-powered regions of the fuel, such as the pellet rim regions (Barner 1985; Guenther et al. 1988). The extent to which the metallic fission products, cesium, and iodine migrate depends on the fuel burnup, operating temperatures, and temperature gradients, as determined by the fuel's linear power history in the reactor (Guenther et al. 1988). Figure 1 shows the key microstructural regions of UO_2 used fuel that influence degradation and radionuclide release.

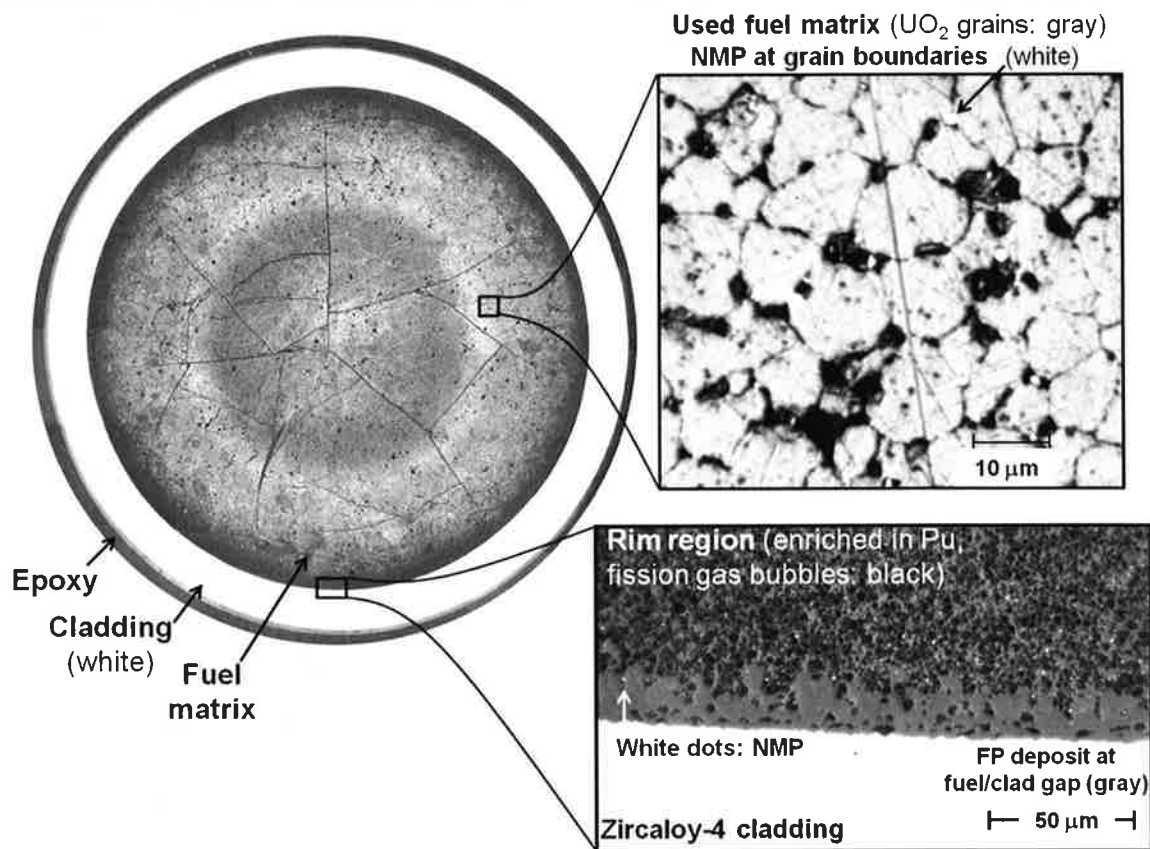


Figure 1. Optical micrographs of a polished used fuel cross-section showing the distinct microstructural regions that influence degradation and radionuclide release (Tsai 2003). This sample was cut from an H. B. Robinson PWR Rod with a burnup of 67 GWd/MTU.

1.3. Fuel Matrix Degradation Process

On the basis of the above discussion, the inventory of each radionuclide can be subdivided into four fractions:

- The gap inventory
- The grain boundary inventory
- The matrix inventory
- The noble metal particle inventory

and the release of radionuclides from each fraction modeled separately. Radionuclides in the gap inventory are immediately made available for transport once a waste package and fuel rod

cladding have been breached (e.g., Shoesmith, 2000). Degradation of the fuel matrix is the first step leading to mobilization of the matrix, grain boundary, and noble metal particle inventory fractions. The principal degradation process when used fuel is contacted by an in-package solution is either oxidative or chemical dissolution. The rate of dissolution of multivalent elements such as uranium and plutonium (of which the used fuel matrix is composed) depends on their oxidation state and hence the electrochemical potential at the dissolving surface. Oxidative dissolution of the fuel leads to rapid degradation and radionuclide release relative to chemical dissolution. For example, the experimental results from Röllin et al., 2001, show that the rate of UO₂ fuel matrix dissolution is nearly three orders of magnitude higher for oxidative dissolution than for chemical dissolution (Figure 2). Chemical dissolution of used fuel is orders of magnitude slower than oxidative dissolution (Figure 2) because the rate is determined by the solubility of UO₂ and PuO₂ (which are refractory ceramics) and diffusion of dissolved uranium and plutonium away from the surface (a process that is slowed by low dissolved concentrations).

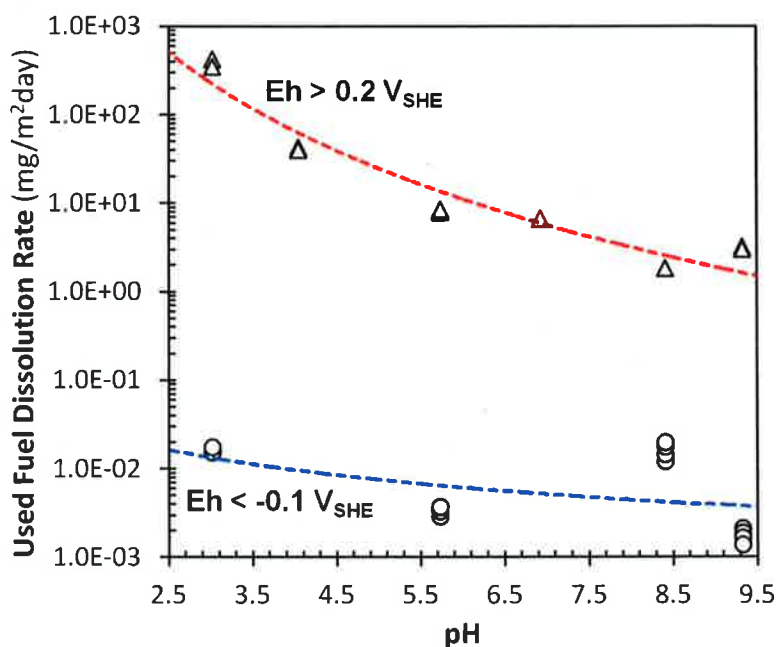


Figure 2. Experimental results from Röllin et al., 2001 showing that the dissolution rate of the UO₂ matrix of used fuel decreases by nearly three orders of magnitude when chemical dissolution vs. oxidative dissolution is the dominant degradation process.

Which mode controls the degradation of used fuel, chemical or oxidative dissolution, is determined by the electrochemical potential at the used fuel/solution interface. This potential is determined by the state of the exposed used fuel and the chemistry of the solution contacting it. The degradation rate model implemented as part of the present study accounts for both chemical and oxidative dissolution. The key processes involved in chemical and oxidative dissolution of used fuel are summarized in Figure 3 which is adapted from Shoesmith, 2007.

The chemical dissolution rate is independent of the electrochemical potential, but depends on the temperature, solution pH, and solution concentrations of complexants and dissolved uranium. The chemical dissolution rate can be calculated using a reaction affinity expression and added to the oxidative dissolution rate calculated with ANL-MPM.

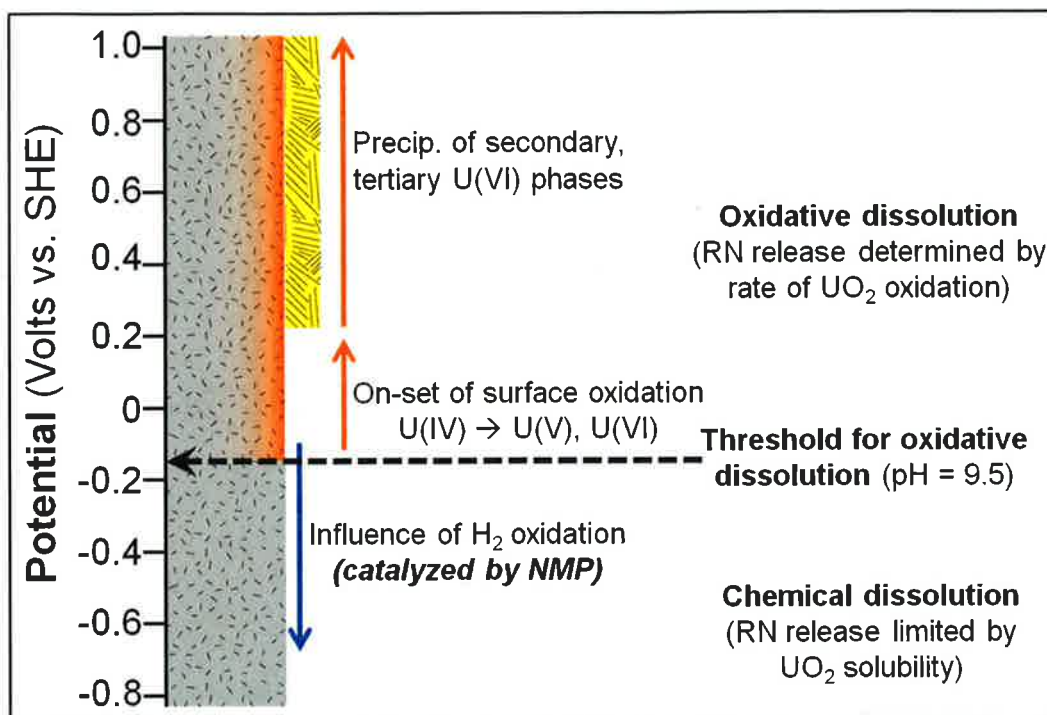


Figure 3. Schematic diagram identifying key surface processes involved in the degradation of used fuel (adapted from Shoesmith, 2007).

Under sufficiently low electrochemical potential conditions, the fuel matrix will not be oxidized upon solution contact and both the fuel dissolution rate and the radionuclide solubilities are low. Under more oxidizing electrochemical conditions, fuel components at the surface can be oxidized to higher oxidation states that are more soluble and dissolve faster. For a given set of physical and chemical conditions, one can define an electrochemical threshold above which oxidative dissolution processes dominate (Figure 3). This refers to the potential at the used fuel surface,

Because the uranium and plutonium atoms in the uranium oxide (UOX) and mixed oxide (MOX) fuels are initially in the (IV) valence state, the electrochemical steps in the used fuel degradation mechanism involve atoms (ions) in the fuel matrix giving up electrons and dissolving into the solution, with the electrons migrating to locations where they are consumed by reduction reactions of oxidizing agents. These oxidizing agents are species that are reduced to “complete the circuit” and maintain electrical neutrality in the system. Relevant reduction reactions include:



The reactants and reaction products have to be transported (e.g., by diffusion or advection) to and from the locations where the oxidation/reduction reactions can occur and, depending on the local micro-chemical environment at the surface of the corroding metal, the oxidized species and the reduced oxidizing agents may undergo hydrolysis, participate in complexation and precipitation/co-precipitation reactions, and/or dissolve into the bulk solution. The electrochemical model implemented as part of the work described in this report accounts for these processes.

Although the radiolysis of groundwater will produce oxidizing agents near the fuel surface that may drive oxidative dissolution even in relatively reducing repository settings, recent results indicate that hydrogen produced by corrosion of the waste package materials (and radiolysis) may be very effective in scavenging the radiolytic oxidizing agents and thereby inhibiting or preventing the oxidation of the fuel (Shoesmith 2007; Poinssot et al. 2004; Nagra 2005). The effect of H_2 to lower the UO_2 corrosion potential (E_{CORR}) below the threshold potential for oxidative dissolution is shown schematically in Figure 3. The limited understanding of this process has limited the credit that is being taken for this effect in current calculations of the performance of spent fuel in geological repositories. Providing a technical basis to support taking credit for this effect is expected to show spent UOX and MOX fuels to be very durable indeed in anoxic repository settings (e.g. Poinssot et al. 2004). The electrochemical model being implemented as part of the work discussed in this report (ANL-MPM Version 2) quantifies the effects of dissolved hydrogen. Current and future work focus on providing a scientific basis and modeling capability for taking credit for the oxidant scavenging effect of hydrogen within the generic repository environments of interest (e.g., granite, basalt, clay/shale, rhyolite, salt). Experimental work is in progress to determine if hydrogen plays an important and long-term role in decreasing the rate of used fuel degradation.

The practical effectiveness of dissolved hydrogen in scavenging radiolytic oxidizing agents has been employed by General Electric Company in their patented NobleChemTM process which is based on injection of hydrogen together with noble metals to scavenge radiolytic oxidizing species in Boiling Water Reactors and thereby reduce the corrosion potential and mitigate stress corrosion cracking issues (Hettiarachchi 2005). Several mechanisms have been proposed to explain the inhibiting effects of hydrogen on the rate of corrosion of UOX and MOX but additional studies are needed to better understand the effect before it can be taken into account in long-term assessments of repository performance (Muzeau et al. 2009).

Figure 3 illustrates the dependence of the UO_2 fuel degradation mechanism on the electrochemical potential at pH 9.5, which represents the carbonate-buffered environment modeled in a Canadian disposal system (adapted from Shoesmith 2007). The range identified as **MPM** in Figure 3 indicates the range of surface potentials predicted by Shoesmith et al. (2003) to occur due to alpha radiolysis in granitic groundwaters. In this example, UO_2 fuel dissolves rapidly by a two-step oxidative dissolution mechanism controlled by the kinetics of oxidation of U(IV) to U(VI) at potentials more positive than -0.16 V. Uranium oxidation does not occur at potentials more negative than -0.16 V under these conditions, so fuel degradation is controlled by the very slow chemical dissolution of the U(IV)-dominated surface at more negative potentials. Whether the electrochemical potential at the surface is greater or less than -0.16 V determines which mechanism is operative under these conditions.

The surface potential is affected by the kinetics of all oxidation and reduction reactions occurring at the fuel surface and the actual threshold value depends on the composition of the fuel and the composition of the groundwater. The competing kinetics of all of the oxidation (anodic) and reduction (cathodic) reactions at the used fuel surface generate a steady state surface potential during the oxidative dissolution process. This potential is referred to as the corrosion potential of the system (E_{CORR}), which is -0.16 V in the example in Figure 3. The actual surface potential at which the mechanism for fuel corrosion changes from (slow) chemical dissolution to (rapid) oxidative dissolution depends on many factors (e.g., pH, T, aqueous speciation, fuel composition) and will differ for each disposal environment. A major goal for our work is to develop a used fuel degradation rate model that quantifies the contributions of all processes to determine the corrosion potential at the used fuel surface for environments of interest. This includes processes that have not been taken into account in other electrochemical models for used fuel degradation, such as the role of (H_2) as a reducing agent and the role surface phases catalyzing redox reactions (e.g., NMP). In addition, the impact of corrosion (of both the fuel and NMPs) and poisons on the catalytic efficiency and long-term degradation behavior is being evaluated.

1.4. Modeling Approach: Implementation of a Mixed Potential Model for Matrix Degradation

To account for the key oxidation/reduction and chemical processes that determine the rate of used fuel degradation a model based on mixed potential theory was implemented. Mixed potential theory is based on two fundamental principles: (1) any electrochemical reaction can be divided into partial oxidation and reduction reactions, and (2) there is no net accumulation of electric charge during the electrochemical reaction (Wagner and Traud, 1938). The first statement has been demonstrated experimentally and the second statement is based on the law of conservation of charge (Bockris and Reddy, 1977). Mixed potential theory has been used to quantify and predict the rate of corrosion of electrical conductors or semi-conductors (e.g., UO_2) by relating the potentials and currents from a number distinct oxidation and reduction reactions occurring simultaneously (e.g., Shoesmith et al., 2003).

The primary advantage of using mixed potential theory as a basis for used fuel degradation modeling is that it captures the fundamental electrochemistry and thermodynamics of the chemical phenomena of interest. Since it is based on fundamentals, such a model is applicable to a wide range of environmental conditions. By using the appropriate parameter values and input variables, the MPM for fuel degradation can be extended to all of the repository concepts being studied as part of the Used Fuel Disposition Campaign.

The mixed potential model that we chose to base our used fuel degradation model on was developed as part of the Canadian nuclear waste disposal research and development program (King and Kolar, 1999, King and Kolar, 2003, Shoesmith et al., 2003). The Canadian model was chosen because it is capable of capturing the fundamental electrochemistry and thermodynamics of the used fuel dissolution process and is versatile enough for application to the full range of repository environments of interest and it can be easily linked to other process models and higher level performance assessment models. The Canadian model is also well-documented and has a well-developed supporting parameter data base. The model described in the above references is

referred to here as the Canadian Mixed Potential Model (Canadian-MPM). Our approach was to first implement the existing Canadian-MPM in our own format using the programming language MATLAB. The language MATLAB was chosen because its modular environment and well-tested equation solvers facilitate the rapid implementation of relatively complex kinetic models. After implementing the MATLAB version of the Canadian-MPM and verifying its accuracy (verification discussed below), we began extending our version (referred to as ANL-MPM) to include additional key redox reactions and processes such as the reduction of hydrogen and the role of NMP as redox reaction catalysts. Our MATLAB implementation of the Canadian-MPM is referred to as ANL-MPM Version 1 and the extended form of the model (i.e., the version that accounts for H_2 and NMP reactions), which is the focus of on-going work, is referred to as ANL-MPM Version 2.

1.5. Canadian Mixed Potential Model (Canadian-MPM)

The Canadian-MPM was developed to predict the corrosion behavior of used fuel inside a failed steel container under anticipated conditions in a granitic repository setting (Shoesmith et al. 2003). This system identifies the solution chemistry, including important solution species that interact with the fuel surface and concentration ranges, the key redox reactions, complexants, potential secondary phases, etc. The approach to modeling the system involves first calculating the electrochemical potential dependences for oxidative dissolution of the UO_2 matrix (anode) and the oxidant reduction (cathodic) half reactions, and then coupling the anodic and cathodic half reactions using the charge conservation constraint (Shoesmith et al. 2003). The Canadian-MPM also accounts for important homogeneous reactions and mass transport processes (diffusion) that are coupled to the heterogeneous reactions occurring at the surface of the corroding UO_2 fuel (Shoesmith et al. 2003).

The physical system being modeled in the Canadian scenario is shown schematically in Figure 4. The diagram on the left of Figure 4 is the initial configuration and the diagram on the right shows the configuration after oxidative corrosion of both the UO_2 fuel and steel canister surface. The used fuel cladding is not accounted for in this model (a conservative assumption). Corrosion of the fuel and the steel result in the formation of porous corrosion layers on each surface that serve as transport barriers which effectively decrease the reactive surface area of the corroding materials. A mathematical description of the model is presented in below.

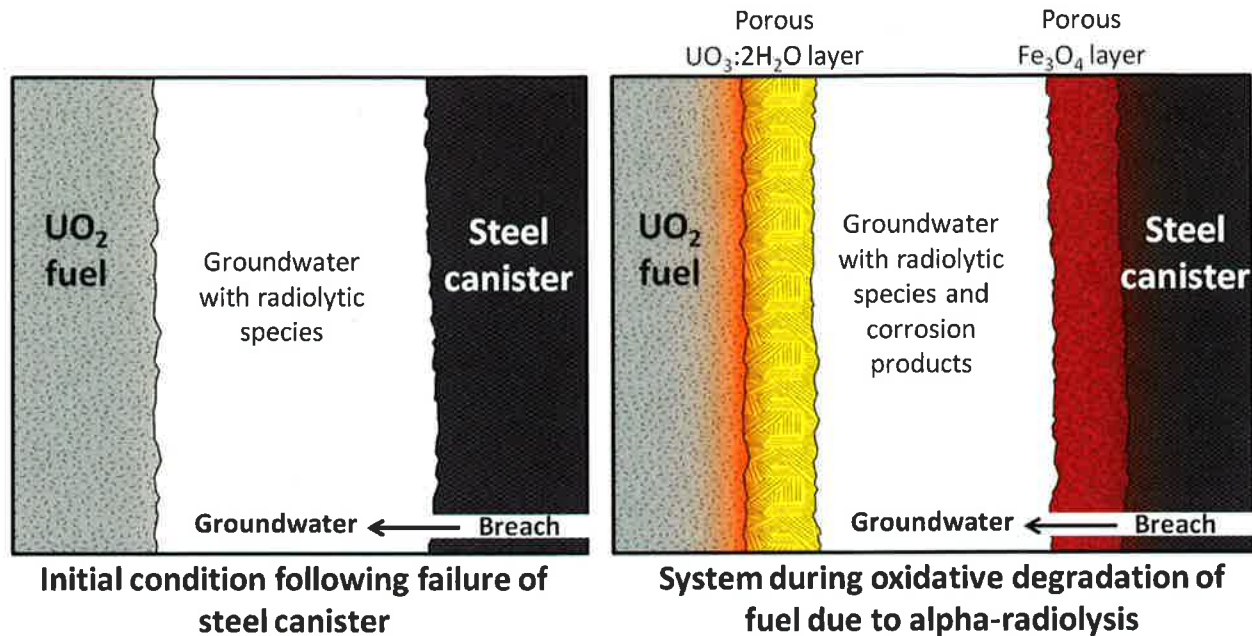


Figure 4. Simplified representation of breached canister system used in Shoesmith et al. (2003) MPM for the oxidative degradation of UO_2 fuel due to alpha radiolysis of water.

The Canadian-MPM is a one dimensional reaction-diffusion model that accounts for both heterogeneous (surface) reactions and homogeneous (aqueous bulk) reactions through a series of mass and charge balance equations. The assumptions on which this model is based are (Shoesmith et al., 2003):

- 1-D model geometry with non-uniform spatial distribution with emphasis on surface reactions at used fuel and steel (Fe) interfaces.
- Uniform dissolution of fuel surface (no localized effects, e.g., grain boundary etching).
- Mass transport by diffusion only.
- System is saturated with groundwater, the supply of groundwater is not limiting.
- Used fuel cladding is excluded from system.
- $\text{U(VI)O}_3 \cdot 2\text{H}_2\text{O}$ and Fe_3O_4 corrosion layers are treated as equivalent porous media with spatially and temporally constant porosity and tortuosity.
- $\text{U(VI)O}_3 \cdot 2\text{H}_2\text{O}$ corrosion layer is assumed to be electrically insulating with electrochemical reactions restricted to areas at base of pores.
- $\text{U(VI)O}_3 \cdot 2\text{H}_2\text{O}$ corrosion layer attenuates alpha dose rate to solution at the fuel surface.
- $\text{U(VI)O}_3 \cdot 2\text{H}_2\text{O}$ corrosion layer may contain alpha-emitting radionuclides (user input).
- Fe_3O_4 is assumed to be the stable corrosion product of carbon steel.
- pH is constant (buffered) throughout system.

The reaction scheme for the Canadian-MPM is shown in Figure 5. The processes accounted for in the model include heterogeneous reactions on the fuel and steel surfaces and homogeneous reactions within the groundwater. Although many more reactions occur, these have been identified as the key reactions in the Canadian disposal system modeled by Shoesmith et al. 2003.

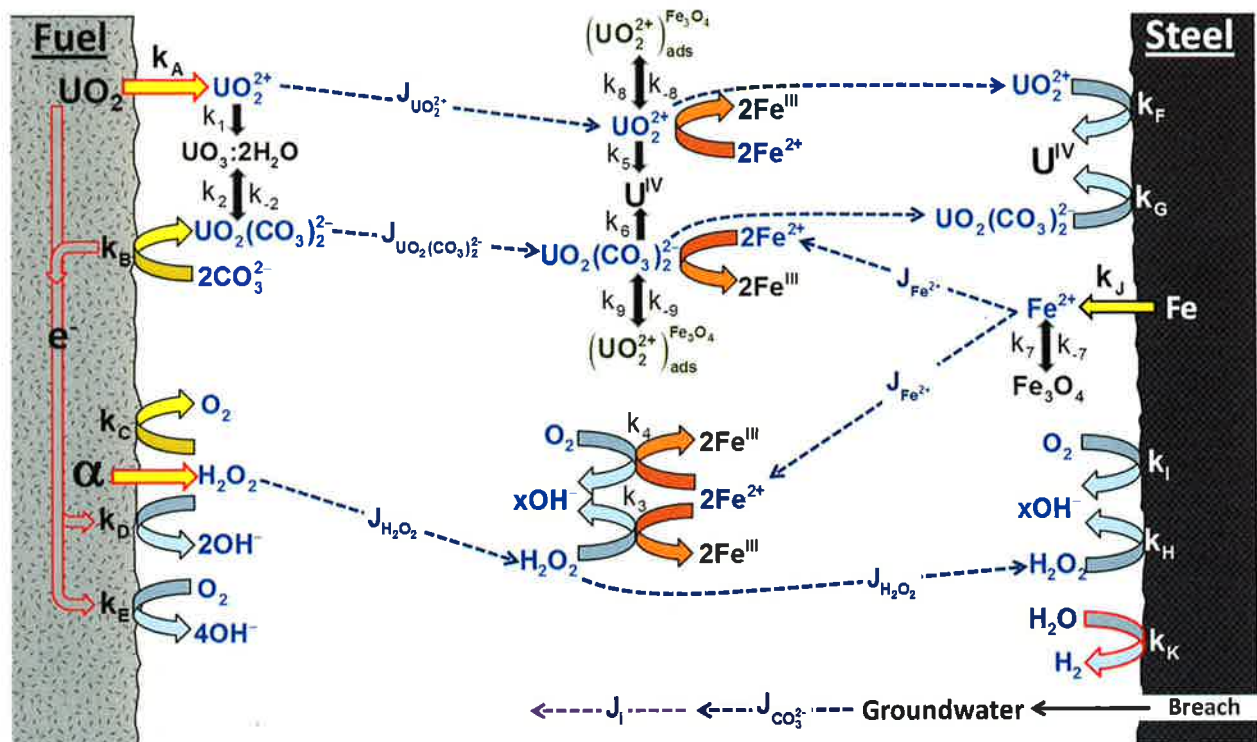


Figure 5. Reaction scheme used in the Shoesmith et al. (2003) (Canadian-MPM) for the oxidative degradation of UO_2 fuel due to alpha radiolysis of water (key half-reactions listed below). Aqueous species are shown in blue, dotted lines represent diffusive fluxes. The “k” labels represent rate expressions for the individual half-reactions. Reactions labeled with letters are for heterogeneous (surface) processes and those labeled with numbers describe homogeneous processes. Anodic reactions are noted with yellow or orange arrows and the cathodic reactions are shown in blue arrows. “ads” stands for adsorbed.

Groundwaters in a granitic repository scenario, such as the Canadian concept modeled by the MPM, will be basic (pH around 9.5), carbonate bearing, anoxic solutions (Shoesmith et al., 2003). Therefore, over the time scales of interest (hundreds to tens of thousands of years), the dominant oxidant will be hydrogen peroxide produced by water radiolysis. In the Canadian-MPM, the dissolved concentration of O_2 is defined by the modeler and the dissolved concentration of H_2O_2 is determined by a radiolysis sub-routine included in the MPM (described below).

1.6. Interface with Generic Performance Assessment Models

The ANL-MPM will provide the fractional matrix degradation rates of used fuel for a specific set of environmental/in-package conditions. These specific environmental conditions will define what ANL-MPM parameter set is used for the used fuel dissolution rate calculation. A library of appropriate parameter sets is the focus of on-going and future experimental work and thermodynamic reaction path modeling (Jerden et al., 2012, Ebert et al., 2012).

The used fuel dissolution rate is calculated on a per surface area basis using the ANL-MPM, where the evolution of the reactive surface area with time is determined by a separate model (e.g., see example discussed in above). The combination of the used fuel dissolution rate from the ANL-MPM and the surface area model is used to determine the overall fractional matrix degradation rate. Source terms for radionuclides are calculated as the product of the fractional degradation rate and radionuclide inventory. Fractional release rates are calculated as the product of the degradation rate and specific surface area.

The used fuel matrix degradation rate and/or the radionuclide source term model results can be treated as direct inputs into the Generic Performance Assessment Model (GPAM). The resulting radionuclide release rates will have a strong scientific basis as they are ultimately based on the fundamental electrochemical and thermodynamic principles underlying the ANL-MPM.

The evolving links for communicating needed inputs/outputs between the ANL-MPM, other EBS process models and the GPAM are discussed in Sassani et al., 2012.

2. ANL IMPLEMENTATION OF THE CANADIAN MIXED POTENTIAL MODEL: ANL-MPM VERSION 1

Based on the work of King and Kolar, 1999, King and Kolar, 2003, Shoesmith et al., 2003 a working version of the Canadian-MPM was implemented by ANL researchers in MATLAB. This model, referred to as the ANL-MPM Version 1, serves as our base-case used fuel matrix degradation model.

As shown in Figures 4 and 5, the Canadian-MPM models the corrosion of both a UO₂ fuel surface and a carbon steel container surface. In the implementation of the ANL-MPM Version 1 we have focused on corrosion of the UO₂ fuel surface, since the purpose of our model is to predict the degradation rate of the used fuel matrix. The ANL-MPM Version 1 does have the built-in capability of modeling steel corrosion; however it is envisioned that canister failure and corrosion will be dealt with in a separate process model within the UFD campaign that will be linked with the ANL-MPM. Therefore, the following discussion of the ANL-MPM deals only with the corrosion of the used fuel surface. For more information on how the steel canister surface is modeled in the Canadian-MPM see King and Kolar, 1999, King and Kolar, 2003, Shoesmith et al., 2003.

2.1. Parameter Database for ANL-MPM Version 1

The core of the ANL-MPM is the parameter database (Tables 1 – 5). Application of the ANL-MPM to disposal scenarios other than granite (base-case scenario for ANL-MPM Version 1) requires optimizing and revising the parameter database to best represent the conditions of interest. The source of parameter values and input variables for the ANL-MPM Version 1 are identified in Tables 1 – 5. This database is currently being optimized using values from recent literature as well as an on-going thermodynamic modeling experimental program involving electrochemical tests that are specifically focused on providing parameter values for the ANL-MPM Version 2 (Jerden et al., 2012, Ebert et al, 2012).

Unless otherwise noted, the parameters listed in Tables 1 - 5 come directly from King and Kolar, 1999, King and Kolar, 2003 (and references therein). Some of the parameter values used in the Canadian-MPM of King and Kolar, 1999 are essentially “place holders” that are based on reasonable assumptions. For example, an activation energy of 6.0×10^4 J/mole is being used for all heterogeneous redox reactions (Table 1) until the temperature dependencies of the individual reactions can be fully quantified by experiment or extracted from existing literature. The initial use of this particular activation energy is justified by the observation that many chemical processes of the type being modeled in the ANL-MPM have measured activation energies around 6.0×10^4 J/mole (e.g., Table 6). Thermodynamic calculations and experimental measurements are being performed to determine if more accurate activation energy values are required based on the sensitivity of the fuel dissolution rate to the temperature. Another important focus of on-going research is identifying and developing links between various process models. For the ANL-MPM, the key links that need to be made (model inputs and outputs) are identified in the concentration column (C_i) of Table 3. This column identifies links to other UFD process models that are being or will be developed as part of the FY-2013 research and development activities (IPC: in-package-chemistry model).

Table 1. Part of the ANL-MPM parameter database: interfacial reactions for UO₂ matrix dissolution. See Figure 4 for coupling between reactions.

Anodic reactions on fuel surface	Reaction label (Fig. 4)	25°C Rate const: K _i (cm/s) or (mol/cm ² s)	Activation energy for k _i : ΔHk _i (J/mol)	Charge Transfer coefficient: α _i	25°C Stand. Pot: E _i ⁰ (V _{SCE})	T dependence of E _i ⁰ : ΔE _i ⁰ (V _{SCE} /K)
UO ₂ → UO ₂ ²⁺ + 2e ⁻	A	5.0E-12	6.0E+04 ^{II}	0.96	0.169	-2.48E-04
UO ₂ + 2CO ₃ ²⁻ → UO ₂ (CO ₃) ₂ + 2e ⁻	B	1.3E-12	6.0E+04	0.82	-0.173	2.10E-03
H ₂ O ₂ → O ₂ + 2H ⁺ + 2e ⁻	C	7.4E-06	6.0E+04	0.41	-0.121	-9.93E-04
H ₂ → 2H ⁺ + 2e ⁻	L	Experiment ^I	Experimental ^I	Experimental ^I	Literature	Literature
Cathodic reactions on fuel surface						
H ₂ O ₂ + 2e ⁻ → 2OH ⁻	D	1.2E-10	6.0E+04	0.41	-0.973	-6.98E-04
O ₂ + 2H ₂ O + 4e ⁻ → 4OH ⁻	E	1.4E-10	6.0E+04	0.50	-0.426	-1.23E-04

I. Electrochemical experiments initiated in FY-2012 are focused on providing parameter values for use in the ANL-MPM, as well as confirming literature values that are currently being used (Jerden et al., 2012).

II. The activation energy of 6.0x10⁴ is being used as a “place-holder” value until these temperature dependencies can be quantified by experiment or identified in existing literature. The use of this particular value is justified by the observation that many chemical processes of the type being modeled in the ANL-MPM have measured activation energies around 6.0x10⁴ J/mol.

Table 2. Part of the ANL-MPM parameter database: homogeneous reactions. See Figure 4 for coupling between reactions.

Homogeneous Bulk Reactions	Reaction label (Fig.4)	25°C Rate const:			Rate const: K_j (cm ³ /mol s)	Activation energy for k_i : ΔH_{ki}^{\ddagger} (J/mol)
		K_i (s ⁻¹)	K_j (mol/cm ² s)	K_j (mol/cm ² s)		
$UO_2^{2+} + 2H_2O \rightarrow UO_3 \cdot 2H_2O + 2H^+$	1	1.0E-03	----	----	6.0E+04	
$UO_2(CO_3)_2^{2-} + 2H_2O \rightarrow UO_3 \cdot H_2O + 2CO_3^{2-} + 2H^+$	2	1.0E-04	----	----	6.0E+04	
$UO_3 \cdot H_2O + 2CO_3^{2-} + 2H^+ \rightarrow UO_2(CO_3)_2^{2-} + 2H_2O$	-2	----	6.3E-16	----	6.0E+04	
$O_2 + 2H_2O + 4Fe^{2+} \rightarrow 4Fe(III) + 4OH^-$	3	----	----	5.9E+05	6.0E+04	
$H_2O_2 + 2Fe^{2+} \rightarrow 2Fe(III) + 2OH^-$	4	----	----	6.9E+04	4.20E+04	
$UO_2^{2+} + Fe^{2+} \rightarrow Fe(III) + U(IV)$	5	----	----	1.0E+04	6.0E+04	
$UO_2(CO_3)_2^{2-} + Fe^{2+} \rightarrow Fe(III) + U(IV) + 2CO_3^{2-}$	6	----	----	1.0E+03	6.0E+04	
$Fe^{2+} + Fe(III) + 4H_2O \rightarrow Fe_3O_4 + 8H^+$	7	1.0E-03	----	----	6.0E+04	
$Fe_3O_4 + 8H^+ \rightarrow Fe^{2+} + Fe(III) + 4H_2O$	-7	----	Function	----	6.0E+04	
$UO_2^{2+} \rightarrow (UO_2^{2+})_{ads}$	8	----	----	1.0E-3	0	
$(UO_2^{2+})_{ads} \rightarrow UO_2^{2+}$	-8	1.0E-06	----	----	----	
$UO_2(CO_3)_2^{2-} \rightarrow (UO_2^{2+})_{ads} + CO_3^{2-}$	9	----	----	1.0E-03	0	
$(UO_2^{2+})_{ads} + CO_3^{2-} \rightarrow UO_2(CO_3)_2^{2-}$	-9	1.0E-06	----	----	----	
$UO_2 + 2H_2O \rightarrow U(OH)_4(aq)$	10	----	1.0E-17	----	6.E+04	
$H_2O_2 \rightarrow H_2O + 0.5O_2$	11	Experimental ¹	Experimental ¹	Experimental ¹	Experimental ¹	

I. Electrochemical experiments initiated in FY-2012 are focused on providing unknown parameter values for the ANL-MPM as well as confirming literature values that are currently being used (Jerden et al., 2012).

II. The activation energy of 6.0×10^4 is being used as a “place-holder” value until these temperature dependencies can be quantified by experiment or identified in existing literature. The use of this particular value is justified by the observation that many chemical processes of the type being modeled in the ANL-MPM have measured activation energies around 6.0×10^4 J/mol.

Table 3. Part of the ANL-MPM parameter database: components (species) included in mass balance equations (see examples Eq.21 – Eq.25). The concentration column (C_i) identifies links to other UFD process models that are being or will be developed as part of the FY-2013 research and development activities (IPC: in-package-chemistry model).

Species	Species Type	Con: C_i (mole/L)	Saturated con: C_i^{sat} (mole/cm ³)	T dependence of C_i^{sat} : ΔH_{sat} (J/mole)	Diffusion coeff. D_i (cm ² /s)	Activation energy ΔH_{Di} (J/mole)
UO ₂ ²⁺	Aqueous	Calculated by ANL-MPM	3.20E-05	6.E+04	5.0E-06	1.5E+4
UO ₂ (CO ₃) ₂ ²⁻	Aqueous	Calculated by ANL-MPM	5.12[CO ₃] ^{1,34}	6.E+04	5.0E-06	1.5E+4
U(IV)	Homogeneous solid	Calculated by ANL-MPM	----	----	----	----
CO ₃ ²⁻	Aqueous	Environmental input (link to IPC)	----	----	1.7E-05	1.5E+4
O ₂	Aqueous	Environmental input (link to IPC)	----	----	1.7E-05	1.5E+4
H ₂ O ₂	Aqueous	Calculated by EBS Radiolysis Model	----	----	1.7E-05	1.5E+4
Fe ²⁺	Aqueous	Environmental input (link to IPC)	1.0E-08	6.E+04	5.0E-06	1.5E+4
H ₂	Aqueous	Environmental input (link to IPC)	----	----	Literature	Literature
U(OH) ₄	Aqueous	Calculated by ANL-MPM	----	----	Literature	Literature
UO ₃ ·2H ₂ O	Homogeneous solid	Calculated by ANL-MPM	Precip. UO ₂ ²⁺ , UO ₂ (CO ₃) ₂ ²⁻	----	----	----
Fe ₃ O ₄	Homogeneous solid	Calculated by ANL-MPM	Precip. Fe ²⁺	----	----	----
Fe(III)	Homogeneous solid	Calculated by ANL-MPM	Precip. Fe ²⁺	----	----	----

Table 4. Part of the ANL-MPM parameter database: physical parameters used in electrochemical and mass balance equations (Eq.1 – Eq.25).

Parameter	Symbol	Value	Units
Porosity of UO ₃ :2H ₂ O layer	ϵ_1	0.45	cm ³ /cm ³
Porosity of bulk solution ^I	ϵ_2	1	cm ³ /cm ³
Faraday constant	F	96487	C/mol
Gas constant	R	8.314	J/K mol
Absolute temperature	T	<i>Input profile</i>	K
Dry density of UO ₃ :2H ₂ O layer	ρ_1	4.98	g/cm ³
Dry density of solution layer ^I	ρ_2	1	g/cm ³
Tortuosity factor of UO ₃ :2H ₂ O layer	τ_1	0.1	----
Tortuosity factor: bulk solution ^I	τ_2	1	----
Reaction order dependence of dissolution rate of UO ₃ :2H ₂ O on [CO ₃]	p	0	----
Reaction order for the dependence of the rate of anodic dissolution of UO ₂ on [CO ₃]	m	6.6E-01	----
Function for dissolution of porous corrosion layer: approximated by finite width profile	δ	<i>Function</i>	----

I. The porosity, density and tortuosity of the bulk solution are specified in the ANL-MPM facilitate the incorporation of porous media into future version of the model (e.g., a porous mass of in-package corrosion products in place of the bulk aqueous solution phase used in the current model).

Table 5. Part of the ANL-MPM parameter database: parameters and variables used in the radiolysis sub-model (see Figures 7 and section 2.4. for discussion).

Parameter	Symbol	Value	Units
G-value for the primary α -radiolysis yield of H_2O_2	$G_{H_2O_2}$	1.02E-10	mol/Gy cm^3
Time-dependent α -radiation dose rate to the solution	$R_{aq}(t)$	Calculated	----
Spatial- and time dependent alpha-radiation dose rate	$R_D(x,t)$	Calculated	----
Ratio of dose rate from U(VI) corrosion layer to dose rate from fuel	R_{film}	0 - 1	----
Geometrical factor describing α -radiation field (see Note below)	$g_f(x)$	Input	----
α -particle penetration depth in water	α_{pen}	35	μm
Scaling factor for dose rate	R_{scale}	1	----

Note:

$$g_f(x) = 1 \text{ if } 0 < x \leq \alpha_{PEN} \text{ and } x_A = 0,$$

$$g_f(x) = 1 + 2R_{film} \text{ if } 0 < x \leq \min(x_A, \alpha_{PEN}),$$

$$g_f(x) = 2R_{film} \text{ if } \alpha_{PEN} \leq x < x_A,$$

$$g_f(x) = \varepsilon + R_{film} (1 - \varepsilon) \text{ if } 0 < x_A \leq x \leq \alpha_{PEN},$$

$$g_f(x) = R_{film} (1 - \varepsilon) \text{ if } \max(x_A, \alpha_{PEN}) < x \leq x_A + \alpha_{PEN},$$

$$g_f(x) = 0 \text{ if } x > x_A + \alpha_{PEN},$$

Table 6. Typical range of activation energy (ΔH) values for selected chemical processes (Langmuir, 1997, page 62).

Reaction or Process	Typical ΔH (kJ/mol)
Physical adsorption	8 - 25
Aqueous diffusion	< 21
Mineral dissolution or precipitation	33 - 151
Mineral dissolution via surface reaction	42-84
Ion exchange	> 84
Isotopic exchange in solution	75 - 201
Solid-state diffusion in minerals at low T	84 - 502

The ANL-MPM Version 1 is based on a set of ordinary differential equations in which concentrations are the state variables. Given initial concentrations of key species (Table 3) at the used fuel surface, a corrosion potential is calculated such that the total current flow at that surface is zero (this is the fundamental axiom of mixed potential theory). The overall rates for all surface reactions are then calculated at that corrosion potential. The rates of the surface reactions control the flux of chemical species from the surface into solution. Species flux from the fuel surface is used to update the concentrations in the solution at the fuel surface. The cycle of calculations is repeated for the desired length of time.

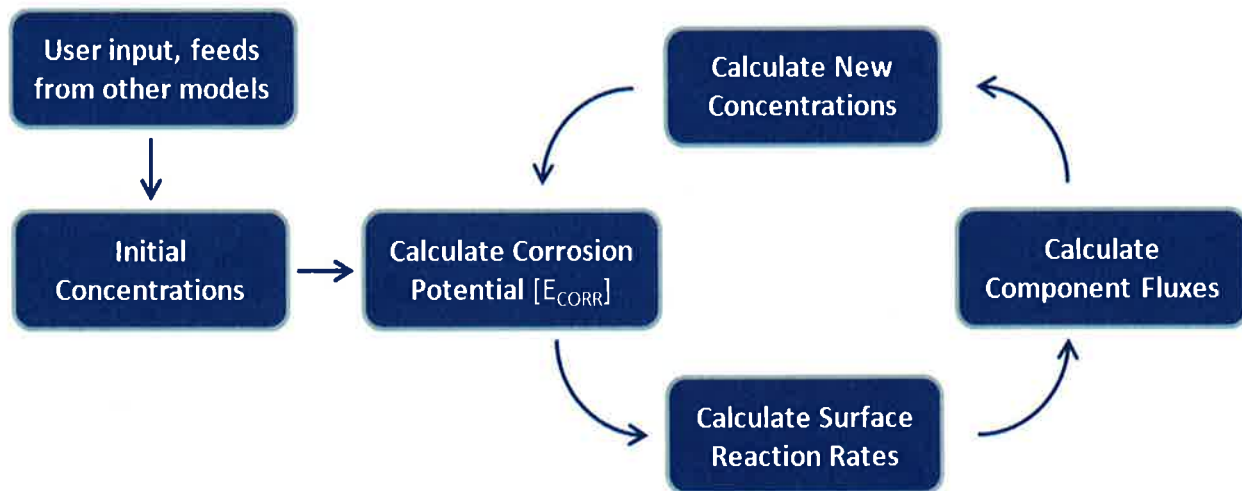


Figure 6. Simplified algorithm for the evolution of the used fuel corrosion potential and interfacial reaction rates with time as calculated by the ANL-MPM Version 1: see Table 3 for concentration input sources.

Implementation of the ANL-MPM is summarized as follows:

- The time derivatives of the species identified in Table 1 were calculated explicitly to reduce the model to a system of ordinary differential equations.
- Several well tested, built-in mathematical tools available in MATLAB were used to facilitate rapid model implementation.
- Modeling systems of partial differential equations like the MPM requires discretization in order to calculate approximate derivative values. The spatial dimension, which is the distance between the used fuel and the steel surface (Figure 5), was divided into multiple cells (the current model uses 250 cells). The cell spacing is logarithmic with finer spacing at the fuel and steel interfaces (Figure 7).
- Placeholder values for physical constants that are not explicitly documented in the Canadian-MPM (e.g., reaction rates and diffusivities) were used to implement the model. The relevant physical constants will be updated based on analyses of literature data and from on-going electrochemical experiments.
- The temperature and radioactive dose profiles are functions of time that are supplied explicitly as an argument to the MPM and are not a result of the calculations (King and Kolar, 1999, King and Kolar, 2003 and references therein).

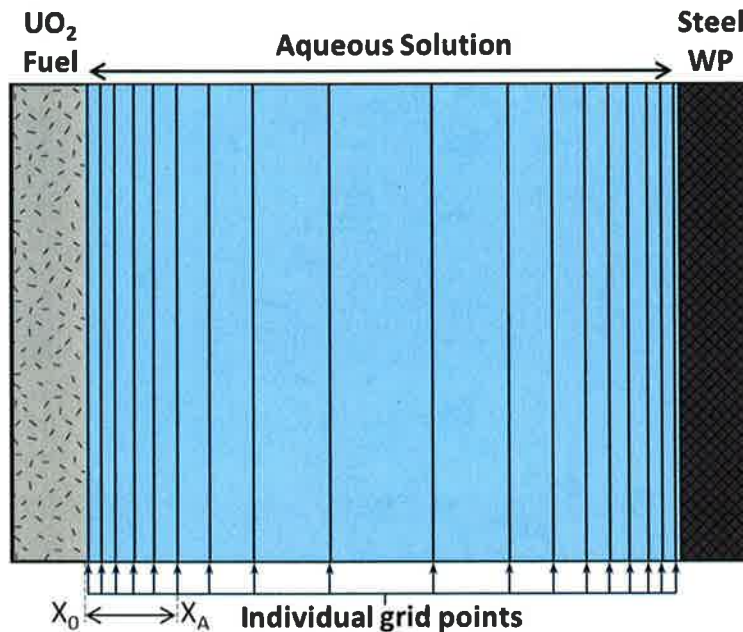


Figure 7. Schematic representation of mixed potential model grid spacing between the used fuel and steel surface boundaries (not all spacings are shown). Spacing is logarithmic with finer intervals at the two interfaces. The current implementation of the ANL-MPM Version 1 contains 250 grid points with a minimum grid spacing of 1 micrometers and a maximum spacing of 1000 micrometers.

The steel waste package is shown to define the spacing and mass transport calculations. The reactions for corrosion of the steel have been implemented into the ANL-MPM Version 1, but the rates are currently set to zero to match available results for the Canadian MPM. It is anticipated that steel corrosion will be modeled separately from fuel degradation in another UFD process model.

The non-electrochemical (chemical) dissolution of the UO_2 matrix (Reaction 10, $UO_2 + 2H_2O \rightarrow U(OH)_4(aq)$, Table 2) is assigned a rate constant of 1×10^{-17} mole/cm²second (King and Kolar, 1999) and its solubility is modeled using saturation concentration of approximately 1×10^{-8} moles/L (King and Kolar, 1999). Due to this low saturation concentration and corresponding slow dissolution rate, the chemical dissolution of the fuel matrix does not represent a significant degradation mechanism in the current model.

2.2. Governing Equations and Fundamental Electrochemical Relationships Used in Mixed Potential Model Implementation

To provide the background needed to fully understand how the ANL-MPM works and thus provide a context for the model results a summary of the governing equations is presented below. Another reason for presenting the equations underlying the ANL-MPM is to show how the parameters described in Tables 1 - 5 are related to each other and thus highlight the parameter values that need to be first priority targets of the on-going experimental program.

In the MPM, the rate of mass loss from the used fuel (a quantification of degradation) is directly related to the corrosion current density by Faradays Law (Equation 1). The corrosion current density is defined as the sum of the current densities of the anodic fuel oxidation reactions (Reactions A and B in Table 1, Equation 2 below).

$$\frac{ML^{Fuel}}{time} = \frac{i_{CORR}^{Fuel} MW^{Fuel}}{nF} \quad (Eq.1)$$

$$i_{CORR}^{Fuel} = i_A + i_B \quad (Eq.2)$$

where $ML^{Fuel}/time$ is the total mass loss rate (grams/m²days) due to oxidative and chemical dissolution, i_{CORR}^{Fuel} is the corrosion current density (amp/m²), MW^{Fuel} is the molecular weight (grams/mole), n is the number of electrons transferred, F is the Faraday constant C/mole). The corrosion current density is related to the used fuel corrosion potential by the Tafel Equation (Equation3).

$$E_{CORR}^{Fuel} = E_A^0 + \frac{RT}{\alpha_A F} \ln \left(\frac{i_{CORR}}{nF \epsilon(SA) k_A} \right) \quad (Eq.3)$$

where E_{CORR}^{Fuel} is the corrosion potential (Volts), E_A^0 is the standard potential for Reaction A (see Table 1), α_A is the electrical charge transfer coefficient (related to Tafel slope for reaction of

interest), ε is the porosity of the U(VI) corrosion layer covering the used fuel surface (m^3 void/ m^3 corrosion phase), (SA) is the reactive surface area of the fuel (m^2), k_A is the rate constant for Reaction A (see Table 1), and R, T, F, n are the ideal gas constant, absolute temperature, Faraday constant and the number of electrons transferred respectively. As implied in Figure 5, the used fuel corrosion potential is also a function (E_0) of the concentrations of species involved in the oxidative dissolution of uranium (see Table 1 for reactions).

$$E_{\text{CORR}}^{\text{Fuel}} = E_0([\text{CO}_3^{2-}], [\text{O}_2], [\text{H}_2\text{O}_2], [\text{H}_2]) \quad (\text{Eq.4})$$

The relationships between reaction currents (directly proportional to reaction rates), rate constants, standard potentials and the corrosion potential for individual half-cell reactions at the used fuel surface (Table 1, Figure 5) are derived from the Tafel equations and quantified as follows:

$$i_A = nF\varepsilon k_A \exp\left[\frac{\alpha_A F}{RT}(E_{\text{CORR}}^{\text{Fuel}} - E_A^0)\right] \quad (\text{Eq.5})$$

$$i_B = nF\varepsilon k_B [\text{CO}_3^{2-}]^2 \exp\left[\frac{\alpha_B F}{RT}(E_{\text{CORR}}^{\text{Fuel}} - E_B^0)\right] \quad (\text{Eq.6})$$

$$i_C = nF\varepsilon k_C [\text{H}_2\text{O}_2] \exp\left[\frac{\alpha_C F}{RT}(E_{\text{CORR}}^{\text{Fuel}} - E_C^0)\right] \quad (\text{Eq.7})$$

$$-i_D = nF\varepsilon k_D [\text{H}_2\text{O}_2] \exp\left[\frac{-\alpha_D F}{RT}(E_{\text{CORR}}^{\text{Fuel}} - E_D^0)\right] \quad (\text{Eq.8})$$

$$-i_E = nF\varepsilon k_E [\text{O}_2] \exp\left[\frac{-\alpha_E F}{RT}(E_{\text{CORR}}^{\text{Fuel}} - E_E^0)\right] \quad (\text{Eq.9})$$

$$i_L = nF\varepsilon k_L [\text{H}_2] \exp\left[\frac{-\alpha_L F}{RT}(E_{\text{CORR}}^{\text{Fuel}} - E_L^0)\right] \quad (\text{Eq.10})$$

where $E_{\text{CORR}}^{\text{Fuel}}$ is the corrosion potential (Volts), E_A^0 is the standard potential for Reaction A (see Table 1), α_A is the electrical charge transfer coefficient (related to Tafel slope for reaction of interest), ε is the porosity of the U(VI) corrosion layer covering the used fuel surface (m^3 void/ m^3 corrosion phase), S is the reactive surface area of the fuel (m^2), k_A is the rate constant for Reaction A (see Table 1), and R, T, F, n are the ideal gas constant, absolute temperature, Faraday's constant and the number of electrons transferred respectively. Note that the equations are written with positive currents for anodic reactions and negative currents for cathodic reactions.

It follows from Equations Eq.1 - Eq.3 that the corrosion current densities for each half cell reaction can also be calculated based on the fluxes of key redox species (Table 3):

$$2i_C + i_E = -nF\tau_f\varepsilon D_{O_2} \frac{\partial C_{O_2}(0,t)}{\partial x} \quad (\text{Eq.11})$$

$$i_C - i_D = -nF\tau_f\varepsilon D_{H_2O_2} \frac{\partial C_{H_2O_2}(0,t)}{\partial x} \quad (\text{Eq.12})$$

$$i_B = -nF\tau_f\varepsilon D_{UO_2(CO_3)_2^{2-}} \frac{\partial C_{UO_2(CO_3)_2^{2-}}(0,t)}{\partial x} \quad (\text{Eq.13})$$

$$i_A = -nF\tau_f\varepsilon D_{UO_2^{2+}} \frac{\partial C_{UO_2^{2+}}(0,t)}{\partial x} \quad (\text{Eq.14})$$

$$i_L = -nF\tau_f\varepsilon D_{H_2} \frac{\partial C_{H_2}(0,t)}{\partial x} \quad (\text{Eq.15})$$

where τ_f and ε are the tortuosity and porosity of the U(VI) corrosion layer, D is the diffusion coefficient and C is the molar concentration, x is the distance from the used fuel surface (Figure 7) and (0,t) refers to the partial derivative of concentration at x = 0 and time = t.

The fundamental axiom on which kinetic mixed potential theory models (such as the ANL-MPM) is thus quantified by the Equation 16 (see Reactions A - L in Figure 5 and Table 1):

$$i_A + i_B + i_L - i_C - i_D - i_E = 0 \quad (\text{Eq.16})$$

The temperature dependence of the used fuel degradation rate is captured in the ANL-MPM using Arrhenius relationships for rate constants (Equation 17), saturation concentrations (Eq.18) and diffusion coefficients (Eq.19). A linear temperature dependency is used for standard electrochemical potentials (Eq.20).

$$k_i = k_i(T_r) \exp \left[\frac{\Delta H_i}{R} \left(\frac{1}{T_r} - \frac{1}{T} \right) \right] \quad (\text{Eq.17})$$

$$C_i^{sat} = C_i^{sat}(T_r) \exp \left[\frac{\Delta H_i^{sat}}{R} \left(\frac{1}{T_r} - \frac{1}{T} \right) \right] \quad (\text{Eq.18})$$

$$D_i = D_i(T_r) \exp \left[\frac{\Delta H_{D_i}}{R} \left(\frac{1}{T_r} - \frac{1}{T} \right) \right] \quad (\text{Eq.19})$$

$$E_i^0 = E_i^0(T_r) + \Delta E_i^0(T - T_r) \quad (\text{Eq.20})$$

where k is a rate constant, T_r is the reference temperature used in determining the activation energy (ΔH) and temperature dependence of the standard potential for a given half-cell reaction (ΔE^0), R is the ideal gas constant, C^{sat} is the molar concentration at which a given corrosion phase precipitates ($UO_3 \cdot 2H_2O$ for corrosion of fuel surface), and D_i is the diffusion coefficient for component i .

A 1-D reaction-diffusion (mass-balance) equation is written for each species tracked in the MPM (see Table 3 for list of species). For example, the concentrations of UO_2^{2+} and H_2O_2 are tracked using the following equations:

$$\begin{aligned} \varepsilon \frac{\partial C_{UO_2^{2+}}}{\partial t} = \frac{\partial}{\partial x} \left(\tau_f \varepsilon D_{UO_2^{2+}} \frac{\partial C_{UO_2^{2+}}}{\partial x} \right) - \varepsilon k_8 C_{UO_2^{2+}} (C_{U(VI)ads}^{max} - C_{U(VI)ads}) \rho + \\ k_{-8} C_{U(VI)ads} \rho - \varepsilon k_5 C_{UO_2^{2+}} C_{Fe^{2+}} - \varepsilon k_1 \max(0, C_{UO_2^{2+}} - C_{UO_2^{2+}}^{sat}) \end{aligned} \quad (Eq.21)$$

$$\begin{aligned} \varepsilon \frac{\partial C_{UO_2(CO_3)_2^{2-}}}{\partial t} = \frac{\partial}{\partial x} \left(\tau_f \varepsilon D_{UO_2(CO_3)_2^{2-}} \frac{\partial C_{UO_2(CO_3)_2^{2-}}}{\partial x} \right) - \\ \varepsilon k_9 C_{UO_2(CO_3)_2^{2-}} (C_{U(VI)ads}^{max} - C_{U(VI)ads}) \rho + k_{-9} C_{U(VI)ads} \rho - \varepsilon k_6 C_{UO_2(CO_3)_2^{2-}} C_{Fe^{2+}} - \\ \varepsilon k_2 \max(0, C_{UO_2(CO_3)_2^{2-}} - C_{UO_2(CO_3)_2^{2-}}^{sat}) + k_{-2} C_{CO_3^2}^p \delta(x-x_A) \end{aligned} \quad (Eq.22)$$

$$\begin{aligned} \varepsilon \frac{\partial C_{CO_3^2}}{\partial t} = \frac{\partial}{\partial x} \left(\tau_f \varepsilon D_{CO_3^2} \frac{\partial C_{CO_3^2}}{\partial x} \right) + \varepsilon k_9 C_{UO_2(CO_3)_2^{2-}} (C_{U(VI)ads}^{max} - C_{U(VI)ads}) \rho - \\ 2k_{-9} C_{U(VI)ads} \rho + \varepsilon k_5 C_{UO_2^{2+}} C_{Fe^{2+}} - 2\varepsilon k_6 C_{UO_2(CO_3)_2^{2-}} C_{Fe^{2+}} + \\ 2\varepsilon k_2 \max(0, C_{UO_2(CO_3)_2^{2-}} - C_{UO_2(CO_3)_2^{2-}}^{sat}) - 2k_{-2} C_{CO_3^2}^p \delta(x-x_A) \end{aligned} \quad (Eq.23)$$

$$\varepsilon \frac{\partial C_{O_2}}{\partial t} = \frac{\partial}{\partial x} \left(\tau_f \varepsilon D_{O_2} \frac{\partial C_{O_2}}{\partial x} \right) - \varepsilon k_3 C_{O_2} C_{Fe^{2+}} \rho - \varepsilon k_5 C_{UO_2^{2+}} C_{Fe^{2+}} \quad (Eq.24)$$

$$\varepsilon \frac{\partial C_{H_2O_2}}{\partial t} = \frac{\partial}{\partial x} \left(\tau_f \varepsilon D_{H_2O_2} \frac{\partial C_{H_2O_2}}{\partial x} \right) + \varepsilon G_{H_2O_2} R_D - \varepsilon k_4 C_{H_2O_2} C_{Fe^{2+}} \quad (Eq.25)$$

where $G_{H_2O_2}$ is the primary α -radiolysis yield of H_2O_2 (mol/Gy cm^3), R_D is the spatial and time-dependent α -radiation dose rate, ε is the porosity of the U(VI) corrosion layer covering the used

fuel surface (m^3 void/ m^3 corrosion phase), ρ is the dry density of fuel and steel corrosion layers (g/cm^3), τ_f is the tortuosity factor for corrosion layers

Similar expressions can be written for other species. One objective of the ANL experimental activity is to identify those species having a significant effect that should be tracked in the model. Most importantly, the mixed potential model of Shoesmith et al. (2003) does not account for the experimentally observed catalysis of $\text{H}_2(\text{aq})$ oxidation on the noble metal particles in used oxide fuel and does not track reactions involving $\text{H}_2(\text{aq})$. Extending the ANL-MPM Version 1 to include the effects of reactions involving $\text{H}_2(\text{aq})$ was the first modifications in the development of ANL-MPM Version 2.

The spatial and time dependent alpha dose rate (R_D) is a function of the parameters described in Table 5. The radiolysis model used to calculate the H_2O_2 source term for the ANL-MPM is discussed in detail in Section 2.5 below. The general equation used to calculate the alpha-dose rate within 10 – 50 micrometers of the used fuel surface and corrosion layer is:

$$R_D(\mathbf{x},t) = R_{\text{scale}} R_{\text{aq}}(t) g_f(\mathbf{x}) \quad (\text{Eq.26})$$

where R_{aq} is the average dose rate received by an aqueous solution in immediate contact with the used fuel, R_{scale} is an arbitrary scaling factor useful for sensitivity calculations and $g_f(\mathbf{x})$ is a geometry factor, which has the following dependence on the distance from the used fuel surface and the presence or absence ($x_A \neq 0$) of the U(VI) corrosion product layer of porosity ϵ and thickness (x_A) (for discussion see Section 2.5 below and Appendix B of King and Kolar, 1999).

2.3. Radiolysis Model Included in the ANL-MPM Version 1

The spatial and temporal dependence of the alpha dose rate shown in Equation 26 is of fundamental significance within the ANL-MPM because, at low concentrations of dissolved oxygen, the only oxidant within the system is the hydrogen peroxide produced by alpha radiolysis. Therefore the rate of matrix degradation in anoxic environments is directly proportional to the alpha dose rate.

Calculating the alpha dose rate (and thus H_2O_2 concentration) for corroding UO_2 fuel is complicated by the effects of U(VI) corrosion products (modeled as schoepite, $\text{UO}_3 \cdot 2\text{H}_2\text{O}$ in ANL-MPM Version 1). A U(VI) corrosion product layer has three effects on the rate of UO_2 degradation:

- Corrosion layer can slow the rate of oxidative dissolution by decreasing the reactive surface area of the fuel.
- Corrosion layer can slow the rate of oxidative dissolution by slowing the rate of diffusion of oxidants (e.g., H_2O_2) to the fuel surface: U(VI) layer is a tortuous porous mass of crystals.
- Corrosion layer can increase the rate of oxidative dissolution if alpha-emitting radionuclides (e.g., actinides) are incorporated into the U(VI) corrosion crystals or occluded within the mass of corrosion products.

All three of these effects are modeled in the ANL-MPM Version 1 by a radiolysis sub-routine that was included within the original Canadian-MPM. Because of dependence of the used fuel dissolution rate on the alpha dose rate the radiolysis sub-routine is described in some detail.

In the ANL-MPM Version 1 alpha-particles are assumed to have a constant energy of 5.3MeV and a solution penetration distance (α_{PEN}) of approximately 35 μm . The modeler can set the penetration distance over the range of $\alpha_{PEN} = 45\mu\text{m}$ for $\sim 6.0\text{MeV}$ alpha-particles down to $\alpha_{PEN} = 10\mu\text{m}$ for $\sim 2.3\text{ MeV}$ particles (King and Kolar, 1999). The quantity of hydrogen peroxide produced by alpha-radiolysis per unit of absorbed dose ($G_{H_2O_2}$) in both models is assumed to be $1.021\text{E-}10\text{ mol/Gy cm}^3$ (Christensen and Sunder 1998).

Fuel corrosion by oxidative dissolution may result in a layer of corrosion products (secondary phases) on the fuel surface, which will affect the rate of continuing degradation. The spatial dependence of the alpha-dose rate and the effects of the corrosion layer on the effective dose rate are taken into account through the factor $g_f(x)$ (King and Kolar, 1999). Three cases are considered: (a) no U(VI) corrosion layer, (b) a corrosion layer thickness (x_A) less than the penetration distance of alpha-particles in solution, and (c) a corrosion layer thickness greater than the alpha-particle penetration distance (i.e., $x_A > \alpha_{PEN}$). These are illustrated schematically in Figure 8. For the ANL-MPM Version 1, the precipitated U(VI) corrosion phase ($\text{UO}_3 \cdot 2\text{H}_2\text{O}$) is modeled as a porous mass containing a series of parallel pores, having a bulk porosity ϵ and an effective pore cross-sectional surface area of $\epsilon(\text{GA})$, where (GA) is the geometrical surface area of the used fuel (King and Betteridge 1998). Future versions of ANL-MPM will account for other uranium oxide fuel corrosion products such as mixed oxides (UO_{2+X}), uranyl peroxides, uranyl silicates and others depending on groundwater/in-package solution chemistry.

In the case of no U(VI) corrosion layer, the solution adjacent to the fuel is irradiated uniformly to a distance equal to α_{PEN} (Figure 8, top diagram).. The dose rate for this scenario is labeled $R_{aq}(t)$. The middle and bottom diagrams of Figure 8 indicate that the presence of an alpha-bearing corrosion product layer leads to the irradiation of a larger volume of solution relative to the no corrosion scenario. If the corrosion layer does not contain alpha-emitting radionuclides then the porous layer acts as a diffusion barrier, slowing the transport of species to and away from the fuel surface.

The pore diameters within the $\text{UO}_3 \cdot 2\text{H}_2\text{O}$ corrosion layer are $< 5\text{ mm}$ (King and Betteridge, 1998). When alpha-emitters are present in the corrosion layer, the solution within the pores is assumed to be uniformly irradiated and the pores are sufficiently widely spaced so that the pore solution is not irradiated by alpha-particles emitted from adjacent pores. The ratio of the dose rates from the U(VI) corrosion layer and the used fuel surface is assumed to be constant and is an input parameter in the ANL-MPM (R_{film}). Thus, the effective dose rate within the pores of the corrosion layer is given by $\epsilon R_{aq}(x,t)(1+2R_{film})$.

In a case where the corrosion layer contains alpha-emitting radionuclides and has a thickness of $x_A \leq \alpha_{PEN}$, three regions are considered:

Region 1 include the solution within the cylindrical pores of the U(VI) corrosion layer which is irradiated by the fuel and the U(VI) phase (Region 1, middle diagram of Figure 8).

Region 2 (middle diagram, Figure 8) is between the surface of the U(VI) corrosion layer and the penetration distance of the alpha-particles, i.e., $x_A < x \leq \alpha_{PEN}$. The solution in this region is irradiated by the exposed used fuel at the base of the pores [effective surface area $\epsilon(GA)$] and by the surface of the U(VI) corrosion layer [effective surface area $(1-\epsilon)(GA)$]. The effective dose rate per unit area in this region, therefore, is $(R_{aq}(x,t)(1-\epsilon)R_{film}$.

Region 3 (middle diagram, Figure 8) is between the distance α_{PEN} and $(x_A + \alpha_{PEN})$. This region of the solution is irradiated by alpha-particles emitted from the surface of the U(VI) corrosion layer that has a surface area of $(1-\epsilon)(GA)$. The effective dose rate per unit area in this region is $R_{aq}(x,t)(1-\epsilon)R_{film}$.

When the U(VI) corrosion layer thickness is greater than α_{PEN} , three irradiation regions are considered (Figure 8, bottom diagram). Within a distance of α_{PEN} , the pore solution is irradiated by both the exposed used fuel surface and by the lower portion of the alpha emitting U(VI) corrosion phase (Region 1, bottom diagram, Figure 8). The effective dose rate in this region per unit geometrical area is $\epsilon R_{aq}(x,t)(1+2R_{film})$. For regions beyond α_{PEN} (i.e., $\alpha_{PEN} < x < x_A$), the pore solution is irradiated only by the pore walls (Region 2, bottom diagram, Figure 8). The effective dose rate per unit geometrical surface area is $2\epsilon R_{aq}(x,t)R_{film}$.

The region of bulk solution within $x_A < x \leq (x_A + \alpha_{PEN})$ is irradiated by the surface of the porous U(VI) corrosion layer of cross-sectional area $(GA)(1-\epsilon)$ (Figure 8, bottom diagram, Region 3). The effective dose rate in this region per unit geometrical surface area is $R_{aq}(x,t)(1-\epsilon)R_{film}$.

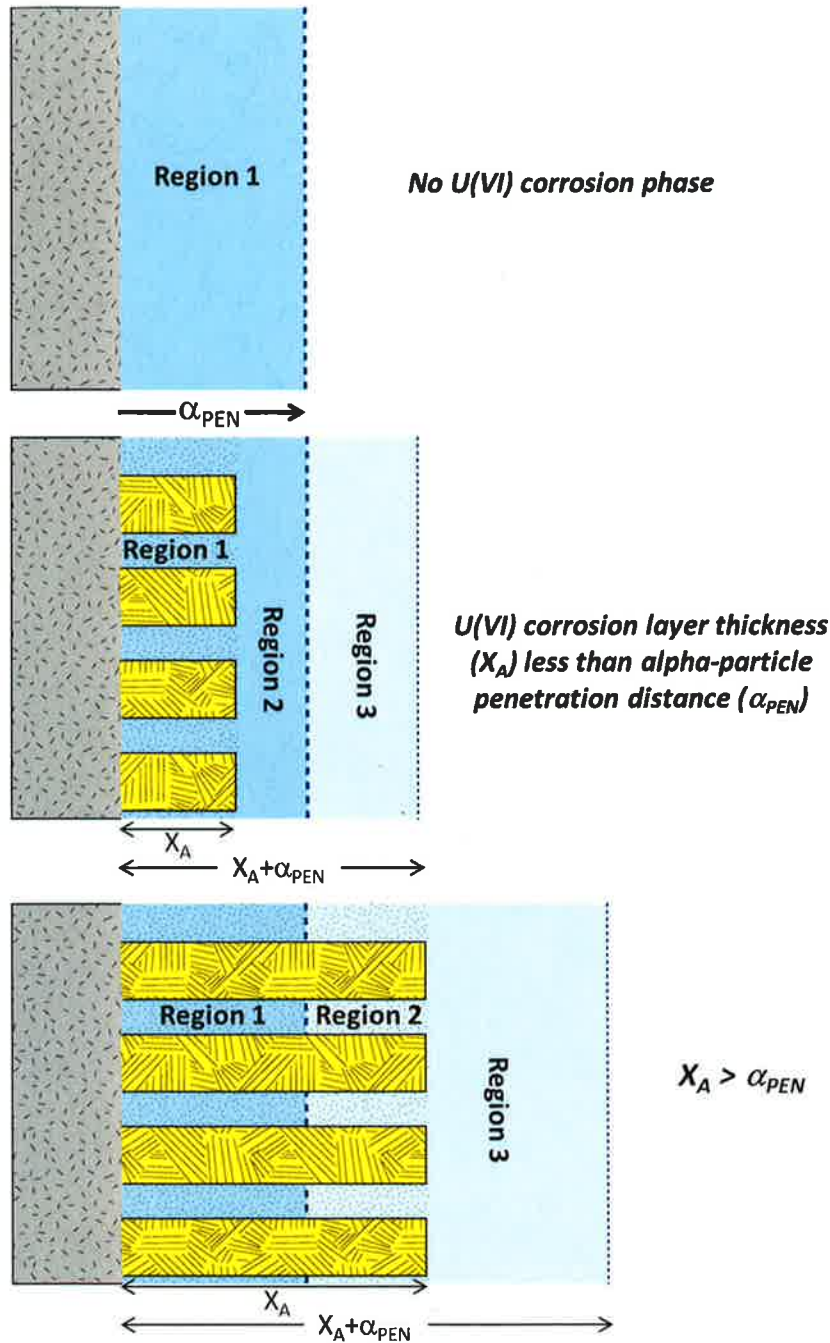


Figure 8. Schematic drawing of the alpha-radiation regions within the ANL-MPM Version 1. See Table 5 and section 2.3. for discussion.

In order to quantify how dose rate influences the fuel dissolution rate, model runs using ANL-MPM Version 1 were performed for a range of absorbed dose, at a constant temperature of 30°C (Figure 9). The plots in Figure 9 are for example calculations made using the parameters shown in Tables 1 - 5 (unless otherwise stated). The top two plots show how the corrosion potential and dissolution rate of the fuel increase with increasing dose rate. For these model runs the starting concentrations of carbonate and dissolved oxygen were 1×10^{-5} molar and 1×10^{-6} molar respectively. The Canadian-MPM assumed a dose profile that varied from approximately 0.02 Gy/s to around 0.002 Gy/s over ten thousand years; however, depending on burn-up and the age of the fuel the dose rate may be considerably higher (King and Kolar, 1999).

The top two plots in Figure 9 indicate that at dose rates lower than 0.01 Gy/s the dissolution rate of the fuel is less than 1 mg/m²day; however, both the corrosion potential and corresponding dissolution rate increase rapidly with increasing dose. For these model calculations the oxidative dissolution of the fuel is driven by the hydrogen peroxide concentration, which is directly proportional to the dose rate (bottom diagrams of Figure 9) (see Eq.26 and Table 5 for relationship between [H₂O₂] and dose rate). The lower left plot in Figure 9 shows concentration profiles of hydrogen peroxide for three different dose rates as well as how the presence of a corrosion layer (UO₃·2H₂O) can affect the concentration profile. The three dose rates 1, 0.1 and 0.01 Gy/s result in hydrogen peroxide concentrations of approximately 7×10^{-7} , 5×10^{-8} and 2.5×10^{-9} moles/L respectively at the fuel surface.

A non-alpha-emitting porous corrosion layer on the fuel surface acts as a diffusion barrier resulting in a steep hydrogen peroxide concentration gradient from the alpha-penetration depth (35 μm) to the fuel surface (Figure 9, lower right plot). The scenario for the blue concentration profile shown in the bottom two diagrams of Figure 9 is analogous to the bottom plot shown in Figure 8 (assuming no incorporation of alpha-emitting radionuclides in the corrosion phase).

The assumption that the U(VI) corrosion phase does not incorporate alpha-emitters is a reasonable if the corrosion layer consists of schoepite (UO₃·2H₂O) (e.g., Friese et al., 2006); however, other types of U(VI) corrosion products such as sodium metaschoepite and uranyl silicates will likely incorporate actinides such as neptunium and plutonium (e.g., Friese et al., 2006). The ANL-MPM is capable of modeling both scenarios (i.e., cases where corrosion layer emits alpha-particles and cases where it does not).

The bottom right diagram in Figure 9 shows that, when the non-alpha-emitting corrosion layer is considerably thicker than the alpha-penetration distance (35 μm for Figure 9), the hydrogen peroxide concentration at the fuel surface is higher than if no corrosion layer was present. This is because the diffusion of hydrogen peroxide away from the fuel surface is slowed by the presence of tortuous pores that are characteristic of the U(VI) corrosion layer (Table 4).

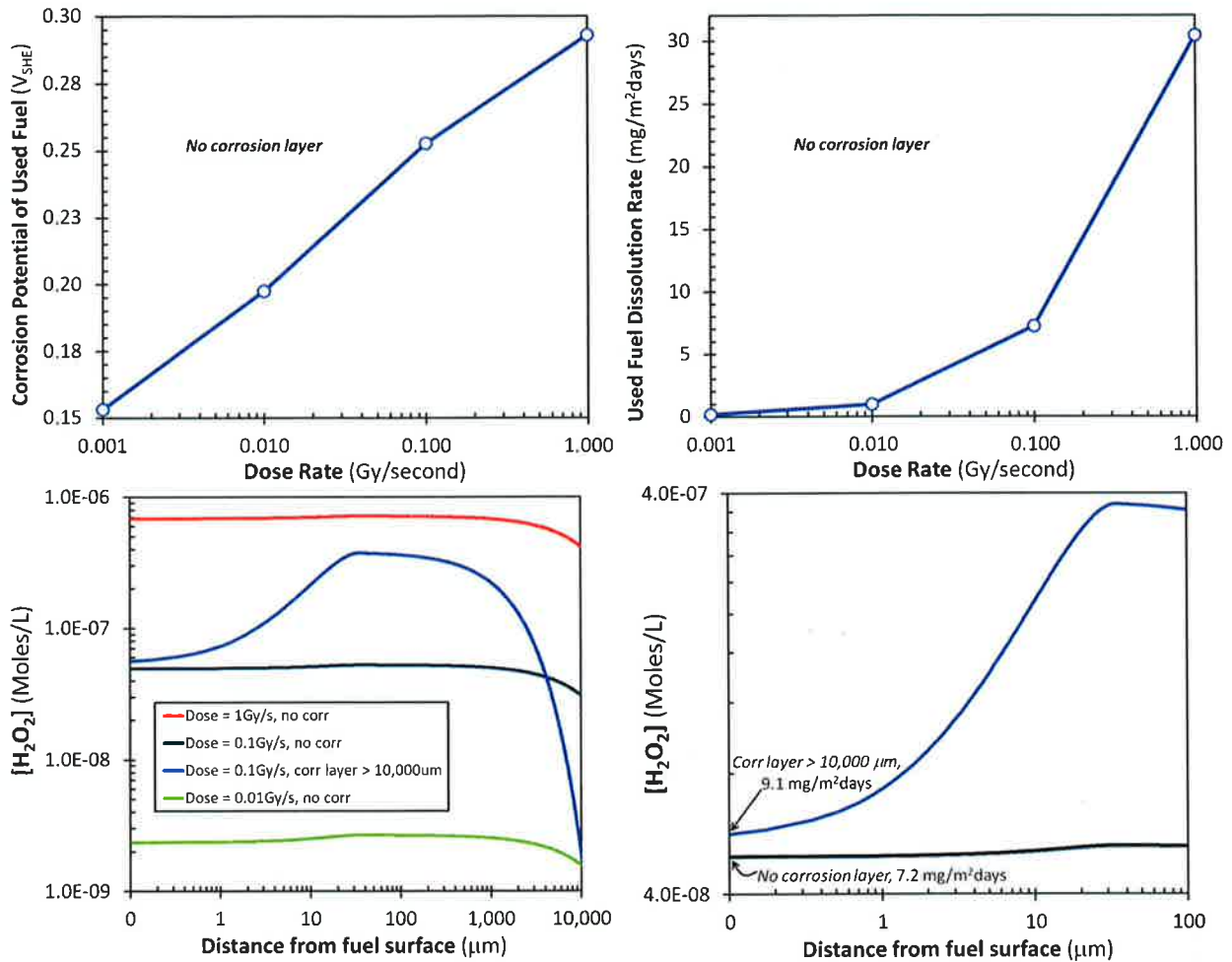


Figure 9. ANL-MPM Version 1 example calculations showing how dose rate and the presence of a U(VI) alteration layer affects the concentration of radiolytic H_2O_2 and the associated fuel corrosion potential and matrix dissolution rate. For these model runs the starting concentrations of carbonate and dissolved oxygen were 1×10^{-5} molar and 1×10^{-6} molar respectively and the temperature was a constant $30^\circ C$.

2.4. Verification of ANL-MPM Version 1 and Sensitivity Studies of Selected Parameters

To confirm that the scripts written in MATLAB for the ANL-MPM Version 1 accurately reproduce the Canadian-MPM documented in King and Kolar, 1999, King and Kolar, 2003, Shoesmith et al., 2003, the ANL-MPM Version 1 was run using the same parameters and input variables that were used to produce Figures 5, 7, 10 and 12 in the Canadian-MPM verification and validation study of King and Kolar, 2002 (see Tables 1 - 5 above for parameters and input variables used).

The comparison of model results from the ANL-MPM Version 1 scripts and those of the Canadian-MPM are shown in Figures 10 - 13. Unless otherwise stated the experimental data

shown in Figures 10 - 13 are from electrochemical tests performed a pH ~ 9 and $\sim 1.0E-4$ molar total carbonate (King and Kolar, 2002).

The comparisons show that, within plotting errors, the ANL-MPM Version 1 reproduces the Canadian-MPM results accurately. Figures 10 – 13 also show examples of some sensitivity studies done with the ANL-MPM Version 1 to identify dominant parameters and input variables. Results from the parameter/variable sensitivity studies are being used to prioritize the on-going electrochemical experimental studies and thermodynamic modeling (Jerden et al., 2012).

In Figure 10, the black curve shows the results of the Canadian MPM and the red dotted curve shows the results from the ANL-MPM Version 1. The curves are identical. The blue curve is from the ANL-MPM Version 1 sensitivity analyses showing how the dissolution rate of UO_2 is affected by the presence of carbonate and the brown curve shows the effect of increasing the temperature. Increasing the carbonate concentration and temperature both significantly increase the predicted dissolution rate.

In Figure 11, the black curves show results of the Canadian-MPM. The top black curve is the dissolution rate calculated using the uranyl and uranyl carbonate species, while the lower black line is calculated using uranyl carbonate only. The dashed blue and red curves show the corresponding results of the ANL-MPM Version 1, which are identical. The solid light blue line (calculated using ANL-MPM Version 1) shows that decreasing the temperature by $25^\circ C$ causes a decrease in the used fuel dissolution rate that ranges from a factor 2x at relatively low carbonate concentrations (1×10^{-4} molar) to a factor of around 1.2x for relatively high carbonate concentrations (1.0 molar).

The black line in Figure 12 shows how the corrosion potential of the UO_2 fuel surface varies with increasing hydrogen peroxide concentration as calculated by the Canadian-MPM. The colored lines were calculated using the ANL-MPM. Again the main point in Figure 12 is that for the same conditions, the ANL-MPM Version 1 accurately reproduces results from the Canadian-MPM (compare black line to red dotted line).

Results from ANL-MPM Version 1 sensitivity runs shown in Figure 12 indicate that the calculated used fuel corrosion potential is sensitive to the hydrogen peroxide concentration for values less than 1×10^{-3} molar. Hydrogen peroxide concentrations greater than 1×10^{-3} molar are not expected in either Canadian or US used fuel disposal systems (King and Kolar, 2002); however, for the sake of comparing the mixed potential model predictions to experimental results, calculations were run for concentration values as high as 0.1 molar (Figure 12). The comparison shows that when the hydrogen peroxide concentration is above 1×10^{-3} molar, the corrosion potential of the fuel reaches a maximum value of around 0.32 volts (SHE). The experimental E_{CORR} values that exceed the MPM predicted E_{CORR} at $[H_2O_2] > 1 \times 10^{-2}$ molar are interpreted to be caused by localized acidification within pores at the fuel surface (King and Kolar, 2002). This type of localized acidification process, which is known to occur under highly oxidizing conditions (Shoesmith, 2000), is not accounted for in the current version of the ANL-MPM Version 1 but may be readily added in future versions of the model if needed.

Figure 13 shows how the ratio of the rates of Reactions C/(A+B) (see Table 1; rates quantified as reaction current densities) varies with increasing hydrogen peroxide concentration. The increase in the oxidation of H₂O₂ (Reaction C) normalized to the overall fuel dissolution rate (Reactions A and B) increases in a nearly linear fashion with the steady state concentration of H₂O₂. This demonstrates that not all of the radiolytic H₂O₂ goes to oxidizing the used fuel, rather, some fraction of the H₂O₂ produced decomposes to produce O₂ at the fuel surface (H₂O₂ → O₂ + 2H⁺ + 2e⁻). When the current density ratio of the hydrogen peroxide oxidation reaction (C) to the uranium oxidation reaction (A+B) exceeds approximately 2, the slope of the curve increases. This increase, which corresponds to the establishment of the E_{CORR} plateau shown in Figure 11, is due to fact that, at this point, most of the total anodic current density is due to H₂O₂ oxidation rather than U(IV) oxidation. The dominance of the H₂O₂ oxidation reaction increases with increasing hydrogen peroxide concentration. As expected, increasing the carbonate concentration decreases the ratio of the rates of Reactions C/(A+B), as increasing [CO₃] increases the rate of Reaction B (the carbonate-aided oxidative dissolution of UO₂).

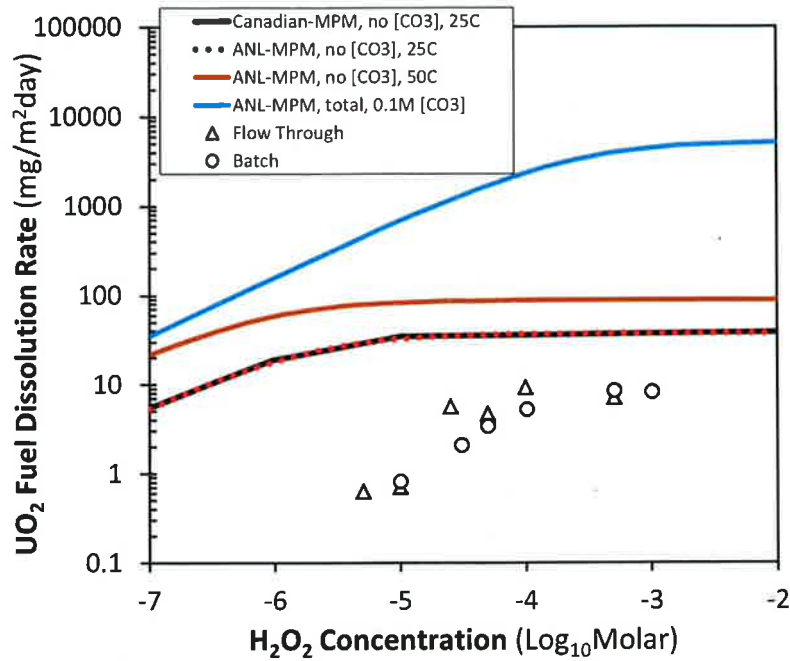


Figure 10. Comparison of results from the ANL-MPM, MATLAB scripts (colored lines) with results from the Canadian-MPM (black line) and experimental results from King and Kolar (2002).

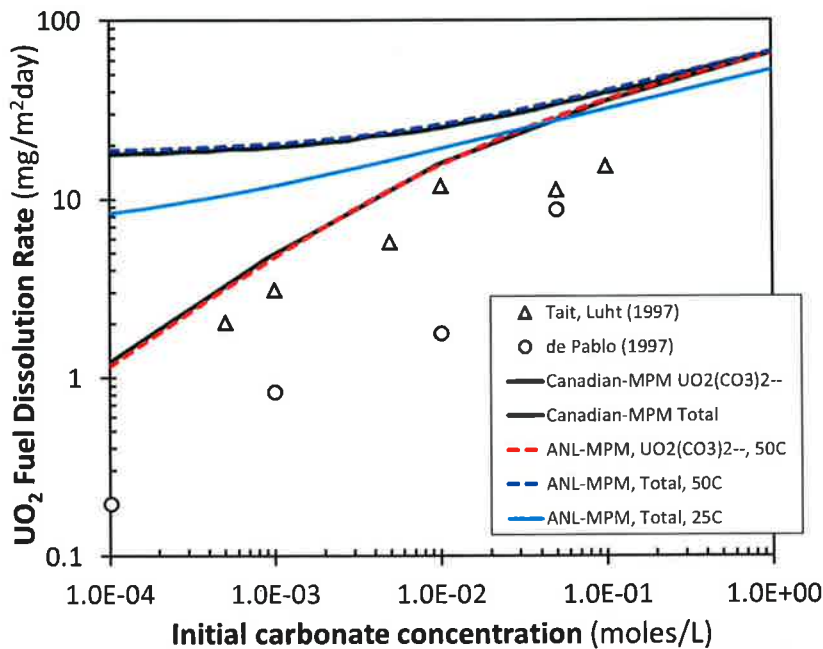


Figure 11. Comparison of results from the ANL-MPM, MATLAB scripts (colored lines) with results from the Canadian-MPM (black lines) and experimental results from King and Kolar (2002).

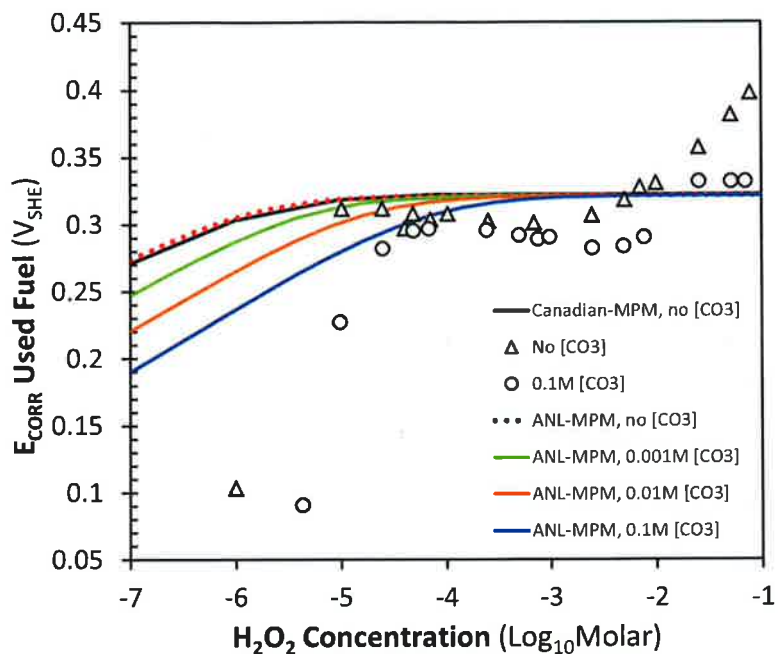


Figure 12. Comparison of results from the ANL-MPM, MATLAB scripts (colored lines) with results from the Canadian-MPM (black line) and experimental results from King and Kolar (2002).

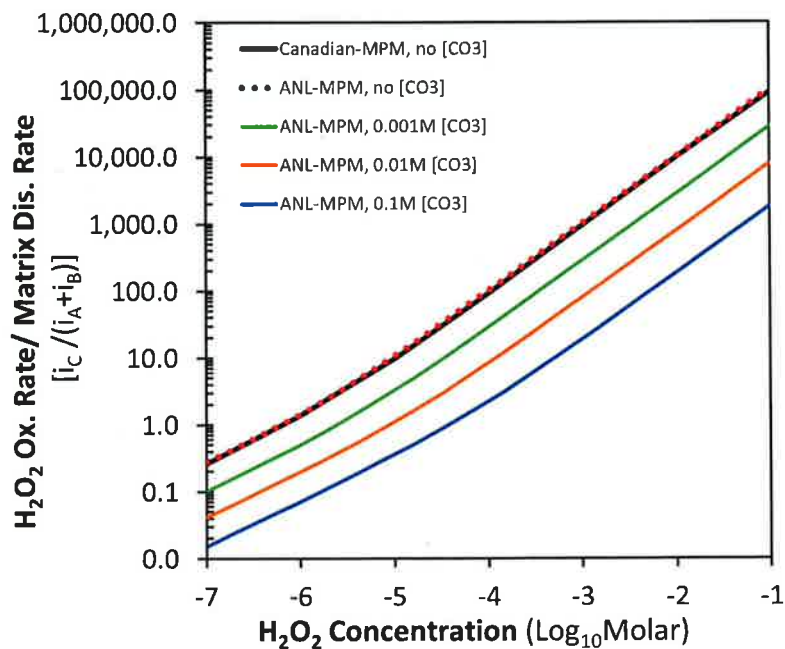


Figure 13. Comparison of results from the ANL-MPM, MATLAB scripts (colored lines) with results from the Canadian-MPM (black line).

2.5. Example Calculation of Used Fuel Matrix Degradation Rate Using the ANL-MPM

The fractional dissolution of the used fuel is calculated based on a dissolution rate provided from the ANL-MPM Version 1 along with an assumed geometry for the fuel matrix. This approach allows flexibility in that the matrix dissolution rate calculation is independent of the fuel assembly and waste package geometry; therefore, a single matrix degradation rate profile may be applied to a number of candidate disposal scenario geometries at low computational cost.

Figure 14 shows an example UO_2 matrix dissolution rate profile that was calculated using the ANL-MPM Version 1 for a 5000 year interval following initial exposure of the UO_2 fuel to a groundwater/in-package solution consisting of 1×10^{-6} molar dissolved oxygen and 1×10^{-3} molar carbonate. The temperature and fuel dose profiles for this example (Figure 15) are assumed to be identical to that of the Canadian repository scenario (King and Kolar, 1999). This assumption was made because the ANL-MPM Version 1 is based on the Canadian-MPM; therefore, reproducing the results from the Canadian studies represents further verification that the ANL-MPM Version 1 accurately reproduces the experimentally validated Canadian code of King and Kolar, 1999, 2002; Shoesmith, 2003.

The matrix dissolution rate (oxidative dissolution of UO_2) in our example is dominated by the rate of reduction of hydrogen peroxide at the UO_2 surface which is strongly temperature dependent. In this model all of the hydrogen peroxide present is produced through alpha-radiolysis (see Section 2.3 above for discussion of how H_2O_2 production is modeled).

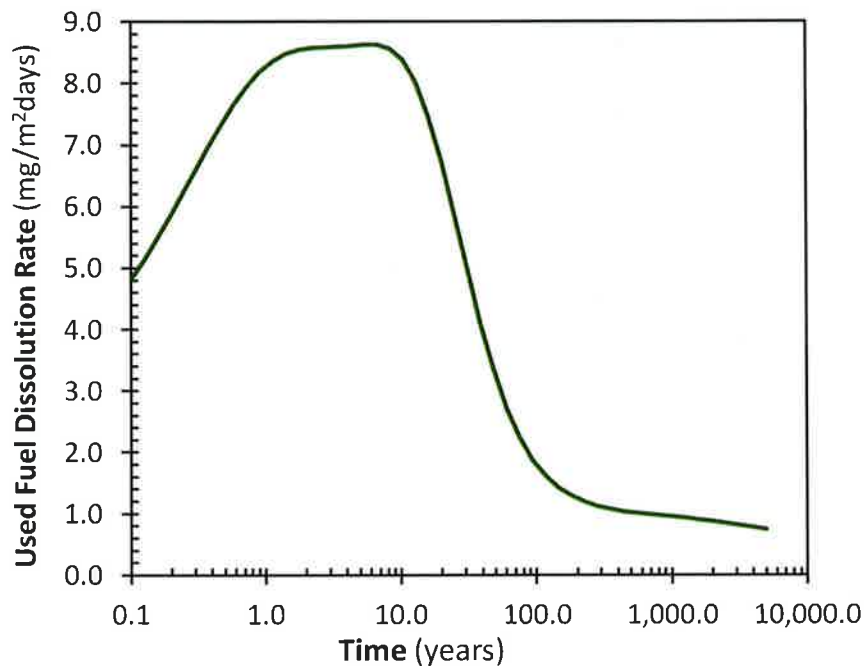


Figure 14. Dissolution rate of uranium dioxide in mg per day per square meter of exposed fuel calculated using the ANL-MPM Version 1 for one millimolar dissolved carbonate (constant) and initial dissolved oxygen concentration of 1×10^{-6} molar. The temperature and dose profiles used for this calculation are shown in Figure 15.

The peak in the predicted used fuel dissolution rate between 1 and 10 years (Figure 14) corresponds to the peak in dose absorbed by the solution within 40 or so micrometers of the used fuel surface and correspondingly to the peak fuel surface temperature (Figure 15). This initial duration (0-100 yr) contributes disproportionately to the total dissolution per area over the 5000 year interval.

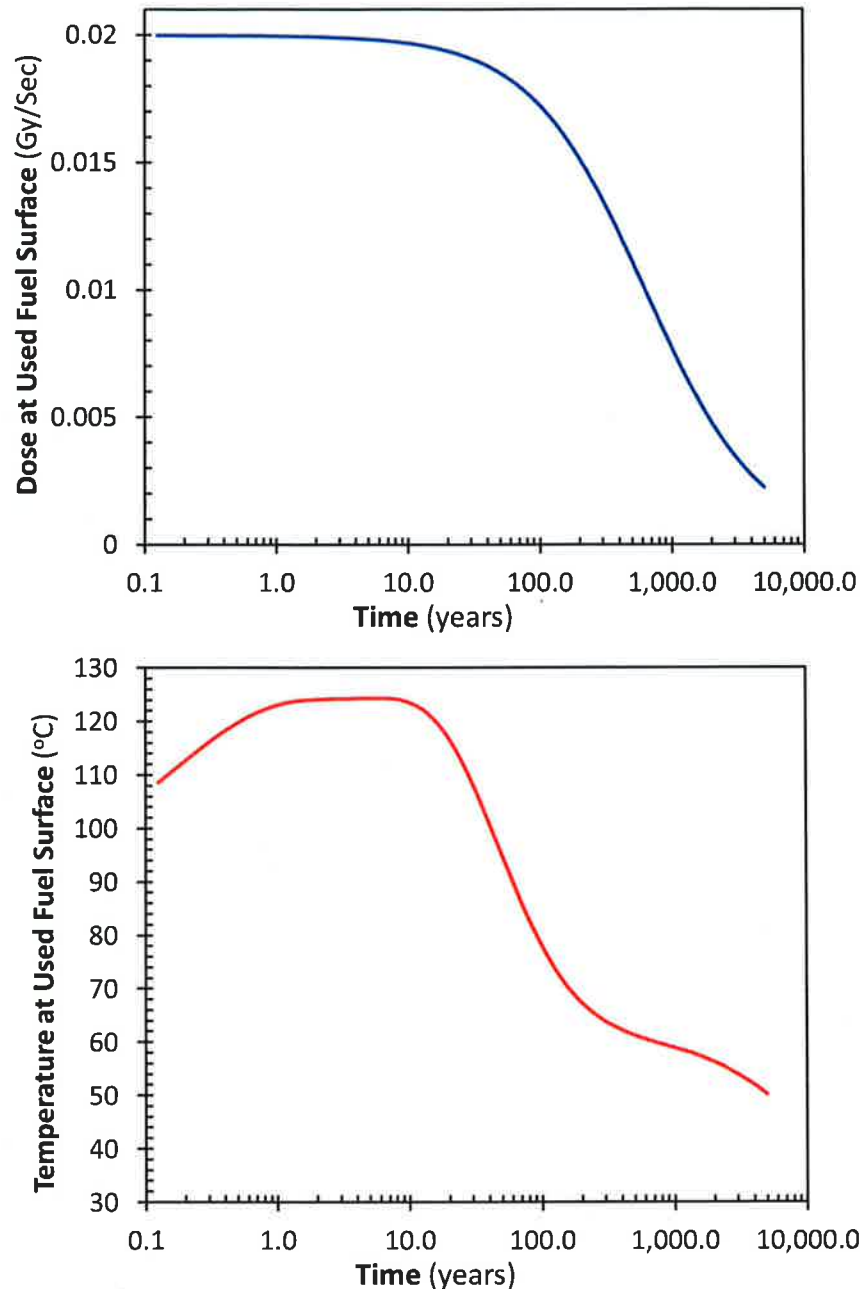


Figure 15. Time dependence of alpha-dose rate in water layer adjacent to used fuel (top) and fuel surface temperature (bottom) used in the example dissolution rate calculation shown in Figure 14. The dose and temperature profiles are from King and Kolar (1999).

2.6. Uncertainty and Conditional Applicability of the ANL-MPM Version 1

The uncertainty in the used fuel degradation model is a propagation of those associated with the conceptual basis of the mixed potential model, the implementation of that model to represent the disposal system and waste materials, including which process variables are explicitly taken into account and the values of model parameters, and the fidelity with which the environment can be represented by those processes and parameter values. Validation of the computer program implementing the model will be considered separately.

The uncertainties associated with the ANL-MPM and associated parameter database have not yet been quantified. At this stage of development, a quantitative uncertainty analysis of the model would be incomplete due to the incompleteness of the ANL-MPM parameter database. As discussed above, the ANL-MPM Version 1 parameter database contains a number of "place holder" values (such as activation energies for temperature dependencies) that are based on reasonable assumptions (see Table 6 and associated discussion). Other parameter values and sources are identified in Tables 1 - 5. Section 3 does, however, lend confidence that the ANL-MPM Version 1 does accurately reproduce the Canadian-MPM (King and Kolar, 2002), which was verified by comparisons to experimental data. Therefore, the ANL-MPM Version 1 is a base-case model with confirmed accurate mathematical implementation, but a somewhat qualitative parameter database. On-going and future work will provide a critically reviewed parameter database for which quantitative uncertainty analyses will be performed for parameter values used in later versions.

Application of the ANL-MPM to different disposal systems will require confirmation that the processes and variables pertinent to the environment are included in the model. It is expected that the different solution compositions in clay, shale, basalt, and salt environments will require the use of different terms and dependencies in the model. Experimental methods are being developed such that key redox and chemical effects on UO_2 dissolution can be systematically identified, evaluated, and quantified for model application.

3. ANL-MPM VERSION 2

A working beta version of ANL-MPM Version 2 is being developed to add redox reactions and expand the modeling capabilities of Version 1 to better represent the disposal environments of interest. The main additions to the ANL-MPM contained in Version 2 are:

- Includes oxidation of dissolved H_2 at the used fuel/solution interface. (The H_2 concentration is supplied by another EBS model or user specified). An important source of H_2 in the disposal system is corrosion of iron-based engineering materials.
- Includes the catalytic NMP (epsilon phase) as a separate domain at the used fuel/solution interface. The relative "size" of the NMP domain is specified by the user as a fractional surface coverage. The NMP domain is electrically coupled with the UO_2 matrix through a user specified electrical resistance that can vary over time to represent corrosion of the NMP and matrix.
- Includes bulk decomposition of hydrogen peroxide (with temperature dependence).
- Includes options for user to specify temperature and dose profiles of the fuel. These profiles can be constant single values or functions (e.g., of time). This provides a link to evolving environmental conditions determined in GPAM calculations.
- Includes a rapid diffusion option to simplify calculation of concentrations of species whose diffusion coefficients are sufficiently large that they reach steady state on the order of days (decreases computer time needed for model convergence). This facilitates modeling long-term behavior, such as the generation of thick alteration rinds and the long-term evolution of radiolysis products.

The conceptual approach for incorporating the catalytic effects of the NMP into the ANL-MPM Version 2 is shown schematically in Figure 17 and the reactions are shown in Table 7. Figure 18 shows a detailed view of the process of interest. As shown in Figure 17 the main new feature of the extended ANL-MPM (Version 2) is the incorporation of the NMP surface as a separate domain at the used fuel/solution interface which is electrically coupled to the used fuel matrix by a user specified resistance. This two domain electrochemical concept is paralleled by the experimental set up we are using to quantify the parameters needed to accurately implement the extended ANL-MPM (Jerden et al., 2012, Ebert et al., 2012).

Figure 16 represents the possible result of the catalysis of H_2 oxidation at the NMP surfaces, specifically, the inhibition of oxidative dissolution of the fuel surface due to rapid reductive destruction of H_2O_2 and aqueous O_2 . This process, which essentially involves the galvanic protection of the fuel by the catalytic behavior of the NMP, is identified as reactions D*, E* and L* in Figure 16.

Table 7. Extension of ANL-MPM parameter database to account for oxidation and reduction reactions that may be catalyzed on noble metal particle surfaces.

Anodic reactions on NMP	Reaction label		25°C Rate const: K_i (s^{-1})	Activation energy for k_i : $\Delta H k_i$ (J/mol)	Charge Transfer coefficient: α_i	25°C Stand. Pot: E_i^0 (V _{SCE})	T dependence of E_i^0 : ΔE_i^0 (V _{SCE} /K)
	C*	L*					
$H_2O \rightarrow O_2 + 2H^+ + 2e^-$	Experiment ¹	Experiment ¹	Experiment ¹	Experiment ¹	Experimental (Tafel analyses) ¹	Literature	Literature
$H_2 \rightarrow 2H^+ + 2e^-$	L*	~0.5 ¹¹	Experiment ¹	Experiment ¹	Experimental (Tafel analyses) ¹	Literature	Literature
Cathodic reactions on NMP							
$H_2O_2 + 2e^- \rightarrow 2OH^-$	D*	~0.5 ¹¹	Experiment ¹	Experiment ¹	Experimental (Tafel analyses) ¹	Literature	Literature
$O_2 + 2H_2O + 4e^- \rightarrow 4OH^-$	E*	Experiment ¹	Experiment ¹	Experiment ¹	Experimental (Tafel analyses) ¹	Literature	Literature

I. Electrochemical experiments initiated in FY-2012 are focused on providing unknown parameter values for the ANL-MPM as well as confirming literature values that are currently being used (Jerden et al., 2012).

II. Calculated from the work of Nilsson and Jonsson, 2008.

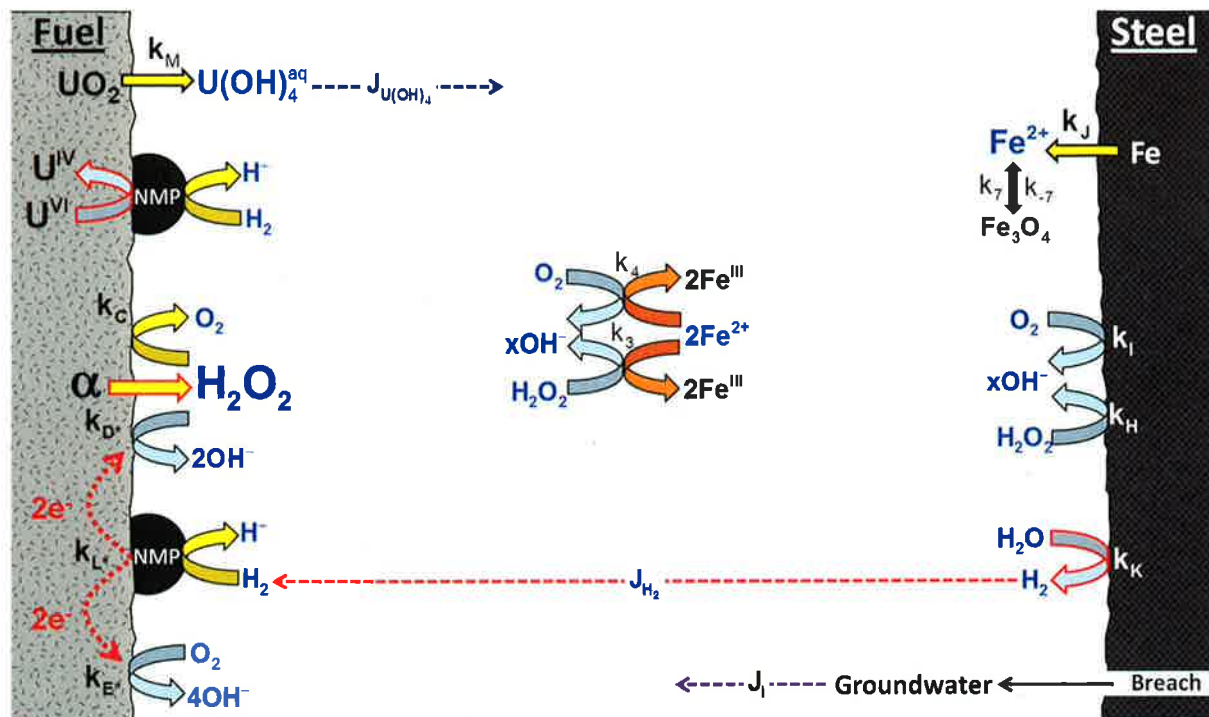


Figure 16. Simplified reaction scheme (not showing all component fluxes) used in the ANL-MPM modified to include catalytic roles of NMP.

The top schematic in Figure 17 highlights the role of the NMP in electrochemically “protecting” the UO_2 fuel from oxidative dissolution. On the right side, electrons released during the oxidation of H_2 on the NMP surface can be used to reduce U(VI) at the surface back to U(IV) and counter the corrosive effect of H_2O_2 reduction in Reaction D. On the left side, the NMP catalyzes the decomposition of H_2O_2 (Reaction D*) to lessen the effect of Reaction D. The lower diagram of Figure 17 illustrates the experimental approach that is being taken to quantify key surface redox phenomena (Table 7, for discussion see Jerden et al., 2012). The NMP and UO_2 materials are physically separated in the experiments to distinguish the currents from reaction at each surface, but are coupled chemically by the common solution and electrically by the potentiostats. Note that Reaction D* will occur in the experiments but not be detected electrochemically. However, the effect of Reaction D* will be detected by any decrease in the dissolution of UO_2 , for example, when the potential on the NMP electrode is increased to slow Reaction L* or when no H_2 is added to the solution.

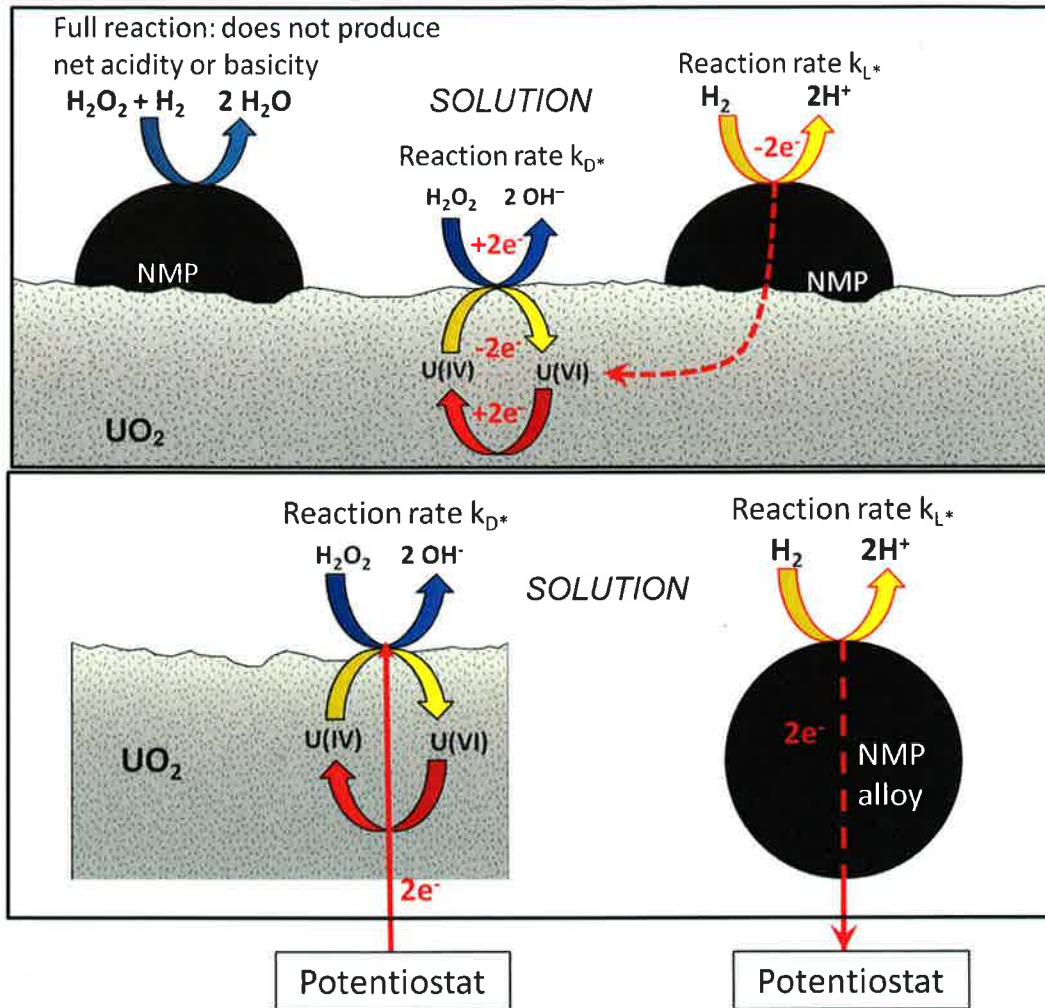


Figure 17. Schematic representation highlighting the process of interest for the ANL study (top) and the basic experimental approach that will be used (bottom).

The ongoing electrochemical experiments (Jerden et al., 2012) involve measuring reaction current densities, corrosion potentials, and released elemental masses from the UO_2 and NMP alloy electrodes under a relevant range of controlled conditions. The experimental results will be used to validate the role of the NMP in the fuel dissolution behavior and determine the form and dependencies of the process model implemented in the module within the ANL-MPM for fuel degradation.

4. SUMMARY AND FUTURE WORK

A used fuel degradation rate model based on fundamental interfacial electrochemistry and thermodynamics is being developed and tested. This model, referred to as the ANL mixed potential model (ANL-MPM), is a 1-D reaction-diffusion code that is based on the mixed potential fuel corrosion model developed as part of the Canadian used fuel repository program (King and Kolar, 1999, 2002; Shoesmith, 2003). The specific objectives for this project that have been achieved this year (FY-2012) and are discussed in this report are as follows:

- Implemented, using our own scripts/code, an established and well documented used fuel degradation model (Canadian-mixed potential model) that is based on mixed potential theory.
- Verified our scripting and coding by reproducing published results from the Canadian model.
- Performed sensitivity analyses to determine which model parameters and input variables have the strongest impact on the calculated used fuel degradation rate.
- Completed a critical review of the sources of all model parameters and input variables to determine which values need further investigation through literature review or experimental studies. This review also identified which variables must be provided by other process models.
- Extended the base-case model to quantify the role of dissolved hydrogen in protecting used fuel from oxidative dissolution by lowering the electrochemical potential at the fuel surface.
- Developed a plan to extend the base-case model to account for the catalytic effects of fission product alloy phase (noble metal particles) on reactions affecting UO_2 dissolution, such as the kinetic balance of H_2 oxidation and H_2O_2 reduction.

The ANL-MPM Version 1 is an implementation of the Canadian-MPM that was prepared to provide a basis for initial sensitivity analyses to guide experiments, to gain hands-on experience to support further refinements of the computing methods, to help in developing approaches for incorporating experimental results, and to serve as a base model for adding modules to include the effects of other reactions and processes. Version 1 accounts for:

- Interfacial redox reaction kinetics (oxidative dissolution of UO_2 matrix).
- Chemical or solubility based dissolution of the fuel matrix
- Complexation of uranium at the fuel surface and in the bulk solution by carbonate.
- The production of hydrogen peroxide (the dominant fuel oxidant in anoxic repository environments) by alpha-radiolysis.
- Diffusion of reactants and products away from and towards the reacting fuel surface.
- The precipitation and dissolution of a U(VI) corrosion product layer on the fuel surface.
- Adsorption of uranium onto iron oxides present in the bulk.
- All interfacial and bulk reactions have a built in Arrhenius-type temperature dependence.

It is anticipated that ANL-MPM Version 1 will be issued in early FY 2013. An initial working beta version of the ANL-MPM Version 2 has been written with modifications to support the

addition of other processes and interactions.. This model version is an extension of the ANL-MPM Version 1 that incorporates the following processes:

- Oxidation of dissolved H_2 at the used fuel/solution interface: H_2 concentration to be supplied by other EBS model or user specified).
- The catalytic NMP (epsilon phase) as a separate domain at the used fuel/solution interface. The relative "size" of the NMP domain is specified by the user as a surface coverage and is electrically linked with the UO_2 matrix by a user specified resistance.
- The bulk decomposition of hydrogen peroxide (with temperature dependence).
- Option for user to specify temperature and dose profiles of the fuel (profiles can be constant single values or functions).
- Rapid diffusion assumption to simplify calculation of concentrations of species whose diffusion coefficients are sufficiently large that they reach steady state on the order of days (decreases computer time needed for model convergence).

Because the ANL-MPM is based on fundamental principles it is flexible enough to be applied to a range of chemical environments. On-going experimental work described in Jerden et al., 2012 and Ebert et al., 2012 is focused on quantifying the key model parameters that are needed to improve predictive accuracy and capabilities such as applying the ANL-MPM Version 2 and future versions to the full range of repository scenarios being considered as part of the UFD campaign (granite, basalt, clay/shale, salt, rhyolite).

Iterative development of the ANL-MPM and supporting experimental work will continue in FY 2013. Activities will include the development analytical expressions for calculating the effects of key environmental variables on the UO_2 dissolution rate—as measured in experiments—within the used fuel degradation model. These effects may include the relative surface areas of UO_2 and NMP, the composition of the NMPs, and quantitative effects of the dissolved H_2 and H_2O_2 concentrations.

REFERENCES CITED AND CONSULTED

- Amme, M. (2002). "Contrary Effects of the Water Radiolysis Product H_2O_2 Upon the Dissolution of Nuclear Fuel in Ground Water and Deionized Water" *Radiochimica Acta*, 90, 399-406.
- Amme, M., B. Renker, B. Schmid, M.P. Feth, H. Bertagnolli and W. Döbelin, (2002). "Raman Microspectrometric Identification of Corrosion Products Formed on UO_2 Nuclear Fuel During Leaching Experiments", *Journal of Nuclear Materials*, 306, 202-212.
- ASTM (2010) *Annual Book of ASTM Standards, Vol. 12.01*, West Conshohocken, Pennsylvania: ASTM-International.
- Barner, J.O. (1985). *Characterization of LWR Spent Fuel MCC-Approved Testing Material-ATM-101*. PNL-5109, Rev. 1. Richland, Washington: Pacific Northwest Laboratory.
- Bethke, C. M., (2009). *The Geochemist's Workbench® Release 8.0 (four volumes)*, Hydrogeology Program, University of Illinois, Urbana, Illinois
- Bethke, C.M., (2008), *Geochemical and Biogeochemical Reaction Modeling*, Cambridge University Press, New York, 543 p.
- Bergel, A., D. Feron, and A. Mollica, (2005). "Catalysis of Oxygen Reduction in PEM Fuel Cell by Seawater Biofilm" *Electrochemistry Communications*, 7, 900-904.
- Broczkowski, M.E., P.G. Keech, J. J. Noel, and D. W. Shoesmith (2010). "Corrosion of Uranium Dioxide Containing Simulated Fission Products in Dilute Hydrogen Peroxide and Dissolved Hydrogen" *Journal of The Electrochemical Society*, 157, C275-C281.
- Broczkowski, M.E., J.J. Noël, D.W. Shoesmith (2007a). "The influence of dissolved hydrogen on the surface composition of doped uranium dioxide under aqueous corrosion conditions" *Journal of Electroanalytical Chemistry*, 602 8-16, (2007)
- Broczkowski, M.E., J.J. Noël, D.W. Shoesmith, (2007b). "The influence of temperature on the anodic oxidation/dissolution of uranium dioxide" *Electrochimica Acta*, 52, 7386-7395 (2007)
- Brokris, J. O'M, and Reddy A.K.N. (1977). "Modern Electrochemistry", John Wiley and Sons, New York.
- BSC (2004). "CSNF Waste Form Degradation: Summary Abstraction" Bechtel SAIC Co. report ANL-EBS-MD-000015 REV02.
- Carbol, P., P. Fors, T. Gouder, and K. Spahiu, (2009a). "Hydrogen suppresses UO_2 corrosion" *Geochimica et Cosmochimica Acta*, 73, 4366-4375.

Carbol, P., P. Fors, S. Van Winckel, and K. Spahiu, (2009b). "Corrosion of Irradiated MOX Fuel in Presence of Dissolved H₂" *Journal of Nuclear Materials*, 392, 45-54.

Casas, I., J. Giménez, V. Martí, M.E. Torrero, and J. de Pablo (1994). "Kinetic Studies of Unirradiated UO₂ Dissolution Under Oxidizing Conditions in Batch and Flow Experiments." *Radiochimica Acta*, 66/77, 23-27.

Choudhary, V.R., C. Samanta, and T.V. Choudhary, (2006). "Factors Influencing Decomposition of H₂O₂ over Supported Pd Catalyst in Aqueous Medium" *Journal of Molecular Catalysis A: Chemical*, 260, 115-120.

Choudhary, V.R., C. Samanta (2006). "Role of Chloride or Bromide Anions and Protons for Promoting the Selective Oxidation of H₂ by O₂ to H₂O₂ Over Supported Pd Catalysts in an Aqueous Medium" *Journal of Catalysis*, 238, 28-38.

Clarens, F., J. De Pablo, I. Casas, J. Giménez, M. Rovira, Merino, J., E. Cera, J. Bruno, J. Quiñones, F. Clarens, A. Martínez-Esparza, (2005). "The oxidative dissolution of unirradiated UO₂ by hydrogen peroxide as a function of pH", *Journal of Nuclear Materials*, 345, 225-231,

Christensen, H. and Sunder, S. (2000). "Current State of Knowledge of Water Radiolysis Effects on Spent Nuclear Fuel Corrosion." *Nuclear Technology*, 131, (1), 102-123.

Cui, D. T. Eriksen, and Ulla-Britt Eklund, (2001). "On Metal Aggregates in Spent Fuel, Synthesis and Leaching of Mo-Ru-Pd-Rh Alloy" *Mat. Res. Symp. Proc.*, 663,

Cui, D., J. Low, C.J. Sjostedt, and K. Spahiu, (2004). "On Mo-Ru-Tc-Pd-Rh-Te Alloy Particles Extracted from Spent Fuel and Their Leaching Behavior Under Ar and H₂ Atmospheres" *Radiochimica Acta*, 92, 551-555.

Cui, D., J. Low, V.V. Rondinella, K. Spahiu, (2010). "Hydrogen catalytic effects of nanostructured alloy particles in spent fuel on radionuclide immobilization" *Applied Catalysis B: Environmental*, 94, 173-178.

Cui, D., J. Low, and K. Spahiu, (2011). "Environmental Behaviors of Spent Nuclear Fuel and Canister Materials" *Energy & Environmental Science*, DOI: 10.1039/c0ee00582g

Cui, D., V.V. Rondinella, J.A. Fortner, A.J. Kropf, L. Eriksson, D.J. Wronkiewicz, and K. Spahiu, (2012). "Characterization of alloy particles extracted from spent nuclear fuel." *Journal of Nuclear Materials*, 420, 328-333.

Cunnane, J.C., J. A Fortner, R. Finch, (2003). "The behavior of light water reactor fuel after the cladding is breached under unsaturated test conditions", *MRS Symposium Proceedings*, 757, 385-392.

Dehaut, P. (2001). "State of the Art of the Oxidation of Spent Nuclear Fuel." in *Synthesis on the Long Term Behavior of the Spent Nuclear Fuel*. Poinssot, C., ed. CEA-R-5958(E). Volume II. Paris, France: Commissariat à l'Énergie Atomique.

DOE (2010). *Next Generation Nuclear Plant*, A Report to Congress prepared by DOE, Office of Nuclear Energy, April 2010.

Ebert, W. L., Cruse, T. A., and Jerden J., (2012), "Electrochemical Experiments Supporting Oxide Fuel Corrosion Model" U.S. Department of Energy Used Fuel Disposition Campaign, Argonne National Laboratory Milestone Report FCRD-UFD-2012-000201

Ekroth, E, O. Roth, M. Jonsson, (2006). "The relative impact of radiolysis products in radiation induced oxidative dissolution of UO_2 ." *Journal of Nuclear Materials*, 355, 38-46.

Eriksen, T. E., Ndalamba, P., Christensen, H., Bjergbakke, E., (1989), Radiolysis of ground water: influence of Carbonate and Chloride on Hydrogen Peroxide Production, *Journal of Radioanalytical and Nuclear Chemistry, Articles*, Vol. 132, No. 1 (1989) 19-35

Eriksen, T. M. Jonsson, J. Merino, (2008). "Modeling of time resolved and long contact time dissolution studies of spent nuclear fuel in 10 mM carbonate solution – A comparison between two different models and experimental data." *Journal of Nuclear Materials*, 375, 331-339.

Ferry, C., C. Poinssot, C. Cappelaere, L. Desgranges, C. Jegou, F. Miserque, J. P. Piron, D. Roudil and J. M. Gras, (2006). "Specific Outcomes of the Research on the Spent Fuel Long-Term Evolution in Interim Dry Storage and Deep Geological Disposal", *Journal of Nuclear Materials*, 352, 246-253.

Ferry, C., J.P. Piron, A. Ambard, (2010). "Effect of Helium on the Microstructure of Spent Fuel in a Repository: An Operational Approach." *Journal of Nuclear Materials*, 407, 100-109.

Fors, P., P. Carbol, S. Van Winckel, and K. Spahiu, (2009). "Corrosion of high burn-up structured UO_2 fuel in presence of dissolved H_2 ." *Journal of Nuclear Materials*, 394, 1-8.

Fortner, J.A., A. J. Kropf, R. J. Finch, and J. C. Cunnane, (2004). "Technetium and Molybdenum in Oxide Spent Nuclear Fuel: Impact on Release Estimates." *Material Research Society Symposium Proceedings*, 824, 107-112.

Freeze, G., P. Mariner, J. Houseworth, J. Cunnane, and F. Caporuscio (2010). "Used Fuel Disposition Campaign Features, Events, and Processes (FEPs): FY10 Progress Report", August 2010.

Friese, J. I., Douglas, M., Jerden, J. L., (2006), Neptunium Association with Selected Uranyl Phases Anticipated in the Yucca Mountain Repository, pp 293–312, in *Separations for the Nuclear Fuel Cycle in the 21st Century*, Editors: Gregg J. Lumetta, Kenneth L. Nash, Sue B. Clark, Judah I. Friese, Volume 933, June 09, 2006, American Chemical Society

Gauthier-Lafaye, F. and P. L. Blanc, (2006). "Natural fission reactors in the Franceville basin, Gabon: A review of the conditions and results of a 'critical event' in a geologic system." *Geochimica et Cosmochimica Acta*, 60, p 4831-4852.

Goldik, J.S., H.W. Nesbitt, J.J. Noël, D.W. Shoesmith, (2004). "Surface electrochemistry of UO₂ in dilute alkaline hydrogen peroxide solutions." *Electrochimica Acta*, 49, 1699–1709.

Goldik, J. S., J. J. Noël, and D. W. Shoesmith, (2006). "The Effects of Simulated Fission Products in the Reduction of Hydrogen Peroxide on Simulated Nuclear Fuel Electrodes" *Journal of The Electrochemical Society*, 153, E151-E159.

Gouder, T., A. Seibert, L., Havela, J. Rebizant, (2007). "Search for Higher Oxides of Pu: A Photoemission Study", *Surface Science*, 601, L77.

Grambow, B., T. Mennecart, M. Fattahi and B. Blondiaux, (2004). "Electrochemical Aspects of Radiolytically Enhanced UO₂ Dissolution", *Radiochimica Acta*, 92, 603-609.

Grenthe, I., Fuger, J., Konings, R.J.M., Lemire, R.J., Muller, A.B., Nguyen-Trung, C., and Wanner, H. (1992), *Chemical Thermodynamics Volume 1, Chemical Thermodynamics of Uranium* NEA OECD, North-Holland, Amsterdam.

Guillaumont, R. Fanghanel, T. Fuger, J., Grenthe, I., Neck, V., Palmer, D. A., Rand, M. H., Mompean, F. J., Domenech-Orti, C., Ben-Said, K., Illemass, M., (2003). *Chemical Thermodynamics Volume 5, Update on the Chemical Thermodynamics of Uranium, Neptunium, Plutonium, Americium and Technetium: Chemical Thermodynamics of Uranium* NEA OECD, Elsevier Science, The Netherlands, Amsterdam.

Guenther, R.J.; Blahnik, D.E.; Campbell, T.K.; Jenquin, U.P.; Mendel, J.E.; and Thornhill, C.K. (1988). *Characterization of Spent Fuel Approved Testing Material—ATM-106*. PNL-5109-106. Richland, Washington: Pacific Northwest Laboratory.

Haschke, J. M., Allen, T. H., Morales L. A., (2000) "Reaction of Plutonium Dioxide with Water: Formation and Properties of PuO_{2+x}" *Science*, 287, 285

He, H., P. Keech, M.E. Broczkowski, J.J. Noel, and D. W. Shoesmith, (2007). "Characterization of the Influence of Fission Product Doping on the Anodic Reactivity of Uranium Dioxide" *Canadian Journal of Chemistry*, 85, 702-713.

He, H., R. K. Zhu, Z. Qin, P. Keech, Z. Ding, and D. W. Shoesmith (2009a). "Determination of Local Corrosion Kinetics on Hyper-Stoichiometric UO_{2+x} by Scanning Electrochemical Microscopy", *Journal of The Electrochemical Society*, 156, C87-C94.

He, H., Ding, Z., Shoesmith, D. W., (2009). "The determination of electrochemical reactivity and sustainability on individual hyper-stoichiometric UO_{2+x} grains by Raman microspectroscopy and scanning electrochemical microscopy" *Electrochemistry Communications*, 11, 1724–1727.

Heisbourg, G., Hubert, S., Dacheux, N., Purans, J., (2004). "Kinetic and thermodynamic studies of the dissolution of thoria-urania solid solutions." *Journal of Nuclear Materials*, 335, 5 -13.

Hettiarachchi, S. (2005). "BWR SCC Mitigation Experiences with Hydrogen Water Chemistry", *Proceedings of the 12th International Conference on Environmental Degradation of Materials in Nuclear Power System – Water Reactors* –Edited by T.R. Allen, P.J. King, and L. Nelson TMS (The Minerals, Metals & Materials Society), 685-701.

Haygarth, K. S., Marin, T. W., Janik, I., Kanjana, K., Stanisky, C. M., and Bartels, D. M., (2010), Carbonate Radical Formation in Radiolysis of Sodium Carbonate and Bicarbonate Solutions up to 250 °C and the Mechanism of its Second Order Decay, *J. Phys. Chem. A* 2010, 114, 2142-2150

Hossain, M. M., E. Ekeroth, M. Jonsson, (2006). "Effects of HCO_3^- on the kinetics of UO_2 oxidation by H_2O_2 " *Journal of Nuclear Materials*, 358, 202-208.

Jerden, J., Fortner, J., Cruse, T., Cunnane, J. (2011). *Repository Science/Waste Form Degradation & Radionuclide Mobilization*, Prepared for U.S. Department of Energy Used Fuel Disposition Campaign, Argonne National Laboratory Milestone Report M41UF030701 for the work package: FTAN11UF0307, July, 2011.

Jerden, J., Fortner, J., Cruse, T., Frey, K., Ebert, W., (2012). *Experimental Plan for ANL Electrochemical Corrosion Studies*, Prepared for U.S. Department of Energy Used Fuel Disposition Campaign, Argonne National Laboratory Milestone Report FCRD-USED-2012-000, January 6, 2012

Jégou, C., B. Muzeau, V. Broudic, D. Roudil and X. "Deschanel, (2007). "Spent Fuel UO_2 Matrix Alteration in Aqueous Media Under Oxidizing Conditions." *Radiochimica. Acta*, 95, 513-522.

Jenks, G. H. 1979. Effects of temperature, temperature gradients, stress, and irradiation on migration of brine inclusions in a salt repository. ORNL-5526, Oak Ridge National Laboratory, Oak Ridge, Tennessee

Jové Colón, C. F., F. A. Caporuscio, S. S. Levy, H. Xu, J.A. Blink, W. G. Halsey, T. Buscheck, M. Sutton, M. A. Serrano de Caro, T. J. Wolery. Hui-Hai Liu, J. Birkholzer, C. I. Steefel, J. Rutqvist, Chin-Fu Tsang, E. Sonnenthal, (2010). "*Disposal System Evaluation and Tool Development – Engineered Barrier System (EBS) Evaluation*", Sept. 2010.

Johnson, L., Ferry, C., Poinssot, C., Lovera P., (2005). "Spent fuel radionuclide source term model for assessing spent fuel performance in geological disposal. Part I: Assessment of the Instant Release Fraction". *Journal of Nuclear Materials*, 346, 66-77.

Jonsson, M., Nielsen, F., Roth, O., Ekeroth, E., Nilsson, S., and Hossain M. M., (2007). "Radiation Induced Spent Nuclear Fuel Dissolution under Deep Repository Conditions", *Environmental Science and Technology*, 41, 7087-7093.

Kaye, M.H. Lewis, B.J. and Thompson, W.T. (2007). "Thermodynamic treatment of noble metal fission products in nuclear fuel." *Journal of Nuclear Materials*, 366, 8–27.

King, F. and Kolar, M. (1999) "Mathematical Implementation of the Mixed-Potential Model of Fuel Dissolution Model Version MPM-V1.0", Ontario Hydro, Nuclear Waste Management Division Report No. 06819-REP-01200-10005 R00.

King, F. and Kolar, M. (2002) "Validation of the Mixed-Potential Model for Used Fuel Dissolution Against Experimental Data", Ontario Hydro, Nuclear Waste Management Division Report No. 06819-REP-01200-10077-R00.

King, F. and Kolar, M. (2003) "The Mixed-Potential Model for UO₂ Dissolution MPM Versions V1.3 and V1.4", Ontario Hydro, Nuclear Waste Management Division Report No. 06819-REP-01200-10104 R00.

Keech, P.G., Noël, J. J., Shoesmith D. W., (2008). "The electrochemical reduction of hydrogen peroxide on uranium dioxide under intermediate pH to acidic conditions" *Electrochimica Acta*, 53, 5675–5683.

Kelm, M., Metz, V., Bohnert, E., Janata, E., Bube, C., (2011). "Interaction of Hydrogen with Radiolysis Products in NaCl Solution – Comparing Pulse Radiolysis Experiments with Simulations" *Radiation Physics and Chemistry*, 80, 426-434.

Klem, M., and Bohnert, E., 2004, A Kinetic Model for the Radiolysis of Chloride Brine, its Sensitivity against Model Parameters and a Comparison with Experiments, European Commission, 5th Euratom Framework Program Report, Institut für Nukleare Entsorgung, Forschungszentrum Karlsruhe GmbH, Karlsruhe (April, 2004).

Kleykamp, H. (1985). "The chemical state of the fission products in oxide fuels." *Journal of Nuclear Materials*, 131, 221-246.

Kleykamp, H, JO Paschoal, R Pejsa, and F Thummler (1985). "Composition and Structure of Fission-Product Precipitates in Irradiated Oxide Fuels - Correlation with Phase Studies in the Mo-Ru-Rh-Pd and BaO-UO₂-ZrO₂-MoO₂ Systems." *Journal of Nuclear Materials*, 130, 426-33.

Kleykamp, H. (1989). "Constitution and Thermodynamics of the Mo-Ru, Mo-Pd, Ru-Pd, and Mo-Ru-Pd Systems." *Journal of Nuclear Materials*, 167, 49-63.

Kropf, A.J., Fortner, J., Finch, R. J., Cunnane, J. C., and Karanfil C., (2004). "A Bent Silicon Crystal in the Laue Geometry to Resolve Actinide X-Ray Fluorescence for X-Ray Absorption Spectroscopy." *Physica Scripta*, 1-3.

Kubatko, K. H., Helean, K. B., Navrotsky, A., Burns P. C., (2003). "Stability of Peroxide-Containing Uranyl Minerals." *Science*, 302, 1191-1193.

Langmuir, D. (1997) *Aqueous Environmental Geochemistry*, Prentice-Hall, Upper Saddle River, New Jersey, 600 pp.

Lee, J., Lomenech C., (2004). "Towards a common thermodynamic database for speciation models." *Radiochimica Acta*, 92, 811-818.

Lemire, R. J. and Garisto. F., 1989. The solubility of U, Np, Pu, Th and Tc in a geological disposal vault for used nuclear fuel. Atomic Energy of Canada Limited Report, AECL- 10009.

Lemire, R. J., Fuger, J., Nitsche, H., Potter, P., Rand, M. H., Rydberg, J., Spahiu, K., Sullivan, J. C., Ullman, W. J., Vitorge, P., Wanner, H., (2001). *Chemical Thermodynamics Volume 4, Chemical Thermodynamics of Neptunium and Plutonium*, NEA OECD, Elsevier Science, The Netherlands, Amsterdam, 872 pages.

Li, J., Staykov, A., Ishihara, T., and Yoshizawa, K., (2011). "Theoretical Study of the Decomposition and Hydrogenation of H₂O₂ on Pd and Au Pd Surfaces: Understanding toward High Selectivity of H₂O₂ Synthesis" *Journal of Physical Chemistry C* 115, 7392-7398.

Lousada, C., and Jonsson M., (2010). "Kinetics, Mechanism, and Activation Energy of H₂O₂ Decomposition on the Surface of ZrO₂" *Journal of Physical Chemistry C*, 114, 11202-11208.

Merino, J., Cera, E., Bruno, J., Quiñones, J., Casas, I., Clarens, F., Giménez, J., De Pablo, J., Rovira, M., Martínez-Esparza A., (2005). "Radiolytic modeling of spent fuel oxidative dissolution mechanism. Calibration against UO₂ dynamic leaching experiments", *Journal of Nuclear Materials*, 346, 40-47.

Metz V., Loida, A., Bohnert, E., Schild, D., and Dardenne, K., (2008). "Effects of Hydrogen and Bromide on the Corrosion of Spent Nuclear Fuel and γ -Irradiated UO₂(s) in NaCl Brine" *Radiochimica Acta*, 96, 637-648.

Nagra (2005). "Spent Fuel Evolution under Disposal Conditions – Synthesis of Results from the EU Spent Fuel Stability (SFS) Project." Technical Report 04-09.

OECD/NEA/IGSC (2011). *R&D for Geological Repositories – Status and Prospects in NEA Countries* (draft report), March 2011.

Neck, V., Altmaier, M., Fanghänel Th., (2007). "Thermodynamic data for hydrous and anhydrous PuO_{2+x}(s)." *Journal of Alloys and Compounds*, 444-445, 464-469.

Nielsen, F., E. Ekeröth, T. Ee. Erikwen, and M. Jonsson, (2008). "Simulation of radiation induced dissolution of spent nuclear fuel using the steady-state approach. A comparison to experimental data" *Journal of Nuclear Materials*, 374, 286-289.

Nielsen, F. and M. Jonsson (2006). "Geometrical α and β -dose distributions and production rates of radiolysis products in water in contact with spent nuclear fuel", *Journal of Nuclear Materials*, 359, 1-7.

Nielsen, F. and M. Jonsson (2008). "Simulations of H_2O_2 concentration profiles in the water surrounding spent nuclear fuel taking mixed radiation fields and bulk reactions into account" *Journal of Nuclear Materials*, 374, 281-285.

Nilsson S., and Jonsson, M., (2011). " H_2O_2 and radiation induced dissolution of UO_2 and SIMFUEL pellets." *Journal of Nuclear Materials*, 410, 89-93.

Pelletier, M. (2001). "State of the Art on the Potential Migration of Species." Section 5.4 of *Synthesis on the Long Term Behavior of the Spent Nuclear Fuel*. Poinssot, C., ed. CEA-R-5958(E). Volume I. [Paris], France: Commissariat à l'Énergie Atomique.

Poinssot C and C. Ferry eds. (2004). *Spent Fuel Stability under Repository Conditions – Final Report of the European Project*, European Commission contract No. FIKW-CT-2001-00192 SFS.

Poinssot, C., C. Ferry, P. Lovera, C. Jegou, and J.-M. Gras (2005). "Spent fuel radionuclide source term model for assessing spent fuel performance in geological disposal. Part II: Matrix alteration model and global performance". *Journal of Nuclear Materials*, 346, 66-77.

Puranen, A., M. Trummer, and M. Jonsson, (2009). "Can redox sensitive radionuclides be immobilized on the surface of spent nuclear fuel? – A model study on the reduction of $Se(IV)_{aq}$ on Pd-doped UO_2 under H_2 atmosphere", *Journal of Nuclear Materials*, 392, 505-509.

Röllin, S., Spahiu, K., Eklund, U. -B., (2001), Determination of dissolution rates of spent fuel in carbonate solutions under different redox conditions with a flow-through experiment, *Journal of Nuclear Materials*, 297, 231-243.

Römer, J., M. Plaschke, G. Beuchle and J. I. Kim, (2003). "In Situ Investigation of U(IV)-Oxide Surface Dissolution and Remineralization by Electrochemical AFM", *Journal of Nuclear Materials*, 322, 80-86.

Roth, O., S. Nilsson, and M. Jonsson (2006). "Radiation enhanced reactivity of UO_2 " *Journal of Nuclear Materials*, 354, 131-136.

Roth, O. and Jonsson, M. (2008). "Oxidation of $UO_2(s)$ in aqueous solution" *Central European Journal of Chemistry*, 6, 1-14.

Roth, O. and Jonsson, M. (2009). "On the impact of reactive solutes on radiation induced oxidative dissolution of UO_2 ", *Journal of Nuclear Materials*, 385, 595-600.

Rothe, J., Walther, C., Denecke, M.A., and Fanghänel, Th. (2004). "XAFS and LIBD Investigation of the Formation and Structure of Colloidal Pu(IV) Hydrolysis Products." *Inorganic Chemistry*, 43, 4708–4718.

Sassani et al., 2012 "*Integration of EBS Models with Generic Disposal System Models*", U.S. Department of Energy, Used Fuel Disposition Campaign milestone report: M2FT-12SN0806062, September, 7 2012

Samanta, C. (2008). "Direct Synthesis of Hydrogen Peroxide from Hydrogen and Oxygen: An Overview of Recent Developments in the Process" *Applied Catalysis A: General*, 350, 133-140.

Shoesmith, D.W., S. Sunder, M. G. Bailey, and G. J. Wallace (1989). "The Corrosion of Nuclear Fuel (UO₂) in Oxygenated Solutions." *Corrosion Science*, 29, 1115-1128.

Shoesmith, D.W., S. Sunder, and J. C. Tait (1998). "Validation of an Electrochemical Model for the Oxidative Dissolution of Used CANDU Fuel." *Journal of Nuclear Materials*, 257, 89-98.

Shoesmith, D.W. (2000). "Fuel Corrosion Processes Under Waste Disposal Conditions." *Journal of Nuclear Materials*, 282, 1-31.

Shoesmith, D.W., M. Kolar, and F. King (2003). "A Mixed-Potential Model to Predict Fuel (Uranium Dioxide) Corrosion Within a Failed Nuclear Waste Container" *Corrosion*, 59, 802-816.

Shoesmith, D. W. (2007). *Used Fuel and Uranium Dioxide Dissolution Studies – A Review*. NWMO TR-2007-03, July 2007 Nuclear Waste Management Organization, 22 St. Clair Avenue East, 6th Floor, Toronto, Ontario M4T 2S3, Canada.

Shoesmith, D. W. (2008). *The Role of Dissolved Hydrogen on the Corrosion/Dissolution of Spent Nuclear Fuel*, NWMO TR-2008-19, November 2008 Nuclear Waste Management Organization, 22 St. Clair Avenue East, 6th Floor, Toronto, Ontario M4T 2S3, Canada.

Soderholm, L., P. Almond, S. Skanthakumar, R. Wilson, and P. C. Burns (2008). "The Structure of the Plutonium Oxide Nanocluster [Pu₃₈O₅₆Cl₅₄(H₂O)₈]¹⁴⁻. " *Angewandte Chemie International Edition*, 47, 298–302.

Sunder, S., N.H. Miller, D.W. Shoesmith, (2004). "Corrosion of uranium dioxide in hydrogen peroxide solutions" *Corrosion Science*, 46, 1095–1111.

Spahiu, K., U.-B. Eklund, D. Cui, and M. Lundström (2002). "The influence of near-field redox conditions on Spent Fuel leaching" *Materials Research Society Symposium Proceedings*, 713, 633-638.

Stumpf S., T. Petersmann, A. Seibert, T. Gouder, F. Huber, B. Brenderbach, and M.A. Denecke, (2010). "Comparative Study of the Structural and Electrochemical Properties of Noble Metal Inclusions in a UO₂ Matrix", *IOP Conference Series: Materials Science and Engineering* 9 012014 (<http://iopscience.iop.org/1757-899X/9/1/012014>)

Suzuki, T., A. Abdelouas, B. Grambow, T. Mennecart and G. Blondiaux (2006). "Oxidation and Dissolution Rates of $\text{UO}_2(\text{s})$ in Carbonate-Rich Solutions Under External Alpha Irradiation and Initially Reducing Conditions" *Radiochimica Acta*, 94, 567-573 (2006)

Torrero, M.E., E. Baraj, J. De Pablo, J. Gimenez, and I. Casas (1997). "Kinetics of Corrosion and Dissolution of Uranium Dioxide as a Function of pH." *International Journal of Chemical Kinetics*, 29, 261-267.

Trummer, M., O. Roth, and M. Jonsson (2009). "H₂ inhibition of radiation induced dissolution of spent nuclear fuel", *Journal of Nuclear Materials*, 383, 226-230.

Trummer, M., B. Dahlgren, and M. Jonsson (2010). "The effect of Y_2O_3 on the dynamics of oxidative dissolution of UO_2 " *Journal of Nuclear Material*, 407, 195-199.

Trummer, M., and Jonsson M., (2010). "Resolving the H₂ effect on radiation induced dissolution of UO_2 -based spent nuclear fuel." *Journal of Nuclear Material*, 396, 163-169.

Tsai, H. (2003). *Personal Communication*, "NRC Review of ANL High-Burnup Cladding Performance Program, July 16, 2003".

UFD R&D Roadmap (2011). *Used Fuel Disposition Campaign Disposal Research and Development Roadmap*. FCRD-USED-2011-000065 REV0, March 2011.

Une, K., S. Kashibe (1996). "Corrosion behavior of irradiated oxide fuel pellets in high temperature water", *Journal of Nuclear Materials*, 232, 240-247.

Utsunomiya S. and Ewing R. C. (2006). "The fate of the epsilon phase (Mo-Ru-Pd-Tc-Rh) in the UO_2 of the Oklo natural fission reactors." *Radiochimica Acta*, 94, 749-753.

Wagner C. and Traud W. (1938). *Elektrochem.* 44, 391.

Wolery, T.J. and Daveler S. A. (1992). *EQ6, A computer program for reaction path modeling of aqueous geochemical systems: Theoretical manual, user's guide, and related documentation (Version 7.0)*. Lawrence Livermore National Laboratory Report UCRL-MA- 110662 PT IV

Wronkiewicz, D.J., C.S. Watkins, A.C. Baughman, F.S. Miller, S.F. Wolf. (2002). "Corrosion Testing of a Simulated Five-Metal Epsilon Particle in Spent Nuclear Fuel" *Materials Research Society Symposium Proceedings*, 713, 625-632.